Studying lateral mobility of surface molecules on the plasma membrane using biophysical approaches

Yun Chen

A dissertation submitted to the faculty of the University of North Carolina at Chapel Hill in partial fulfillment of the requirements for the Doctor of Philosophy degree in the Department of Biomedical Engineering.

Chapel Hill
2007

Approved by

Advisor: Professor Ken Jacobson, Ph.D.

Reader: Professor Jeffrey M. Macdonald, Ph.D.

Reader: Professor Nancy Thompson, Ph.D.

Reader: Professor David Lalush, Ph.D.

Reader: Professor Mark Tommerdahl, Ph.D.

Abstract

Yun Chen: Studying lateral mobility of surface molecules on the plasma membrane using biophysical approaches

(Under the direction of Ken Jacobson)

Fluorescence recovery after photobleaching (FRAP), fluorescence correlation spectroscopy (FCS) and Single particle tracking (SPT) are common biophysical methods to measure lateral mobility of membrane molecules. These methods typically sample lateral mobility in micron-sized regions of the membrane so that they can be used to measure diffusion in regions of single cells. The methods are based on fluorescence from the molecules of interest or from light scattered from particles attached to single or small groups of membrane lipids or proteins. FRAP methodologies are described for a dedicated wide field microscope, which can be applied to confocval-based FRAP too. SPT can be applied to track single fluorescent molecules in membranes but this aspect will not be treated in detail.

SPT has been a useful tool to study the micro-structure of membranes on various time scales. Using SPT, we found that by deliberately cross-linking several glycosyl-phosphatidylinositol-anchored proteins under antibody conjugated 40-nm gold particles, transient anchorage of the gold-labeled clusters occurred for periods ranging from 300 ms to 10 seconds. This

phenomenon was observed with two different GPI-anchored proteins: Thy-1 and CD73, a 5' exonucleotidase. Cholesterol depletion and Src family kinase (SFK) inhibition abolished transient anchorage, indicating the involvement of cholesterol and SFKs in cross-linking dependent transient anchorage. Further evidence for the involvement of SFKs was obtained from Src, Yes, Fyn defective cells, in which transient anchorage of CD73 was not detected. Caveolin-1 knockout cells exhibited reduced transient anchorage time, suggesting the partial participation of caveolin-1. Additionally, in PI3 kinase inhibited IMR 90 cells expressing CD73, short-period transient anchorage (< 1 second) increased sharply and no long-period anchorage occurred. By contrast, a transmembrane protein, the cystic fibrosis transmembrane conductance regulator, exhibited transient anchorage without deliberately enhanced cross-linking; moreover, it was only slightly inhibited by cholesterol depletion or SFK inhibition and depended on interaction of its PDZ binding domain with the adaptor EBP50. We propose that cross-linked GPIAPs become transiently anchored via a cholesterol dependent, SFK-regulatable linkage between a transmembrane cluster sensor and the cytoskeleton.

Acknowledgement

I thank Dr. Ken Jacobson for his guidance during my study. My gratitude also goes to my family, which is always my strength. I owe my appreciation to many kind people who have helped me professionally or otherwise. Thank you all.

TABLE of CONTENTS

Page

LIST OF TABLE

Table page

LIST OF FIGURES

LIST OF ABBREVIATIONS

CFTR: cystic fibrosis transmembrane conductance regulator

FCS: Fluorescence Correlation Spectroscopy

FRAP: Fluorescence Recovery after Photobleaching

GPIAP: glycosyl-phosphatidylinositol-anchored proteins

RAT: relative anchorage time

SPT: Single Particle Tracking

TCZ: Transient Confinement Zone

Chapter 1: introduction

The dissertation is arranged into 6 chapters. In Chapter 1, an overview of doctoral study is described; introducing the evolution of membrane biology, various approaches studying membrane structures of live cells, and the findings obtained using these methods. In Chapter 2, methods to measure the lateral diffusion of membrane lipids and proteins are described in details, including the instrument configurations and the interpretation of the results obtained by these methods. In Chapter 3, the engineering work to reconfigure the FRAP system is described, where the hardware setup and software designs are detailed. In Chapter 4, Transient confinement Zones detected by single particle tracking are discussed regarding the detection algorithm and the biological significance of transient confinement zones. In Chapter 5, we report a novel feature of lateral movement of cross-linked surface molecules, transient anchorage, detected by single particle tracking. Characterizations of transient anchorage as well as its possible mechanisms are included in the chapter. In Chapter 6, future work is outlined to further explore transient anchorage.

Chapter 2: Overview

The view for the structure of the plasma membrane shifted over the past 15 years from the original fluid mosaic model proposed by Singer and Nicolson (Singer and Nicolson, 1972) to the one emphasizing the lateral heterogeneities in membranes. In the fluid mosaic model, the plasma membrane is depicted as 2-D fluid where lipids, proteins and other membrane components diffuse more or less freely in random motions. Lateral heterogeneity is prominent in the lipid raft model, where it is proposed that there are small entities on the plasma membrane with distinct biochemical/biophysical characteristics, such as viscosity and molecular composition (Simons and van Meer, 1988; van Meer and Simons, 1988). These microdomains, or lipid rafts, are speculated to serve specialized cellular functions. For example, it is proposed that lipid rafts are responsible for conveying signals into the cell from outside the cell upon stimuli, such as ligand binding, oligomerization/cross-linking of surface molecules and entry of pathogens (Simons and Toomre, 2000). The lipid raft model postulates that these small entities are composed of sphingolipids, cholesterol, GPI-anchored proteins and some specific transmembrane proteins. Moreover, these platforms recruit the essential signaling molecules and thus allow the subsequent signal transduction occur effectively in response to the stimulus. Early biochemical studies showed that the putative lipid raft components and signaling molecules in the inner leaflet such as Src Family Kinases (SRC) and

protein kinase C (PKC) could be both found in detergent resistant membrane (DRM) fractions of the cell lysates (Simons and Ikonen, 1997; Simons and Toomre, 2000). In addition, microscopic evidence also showed that microdomains formed upon cross-linking or ligation. Such microdomains not only consisted of the surface molecules being engaged, but also of other molecules which are speculated to be raft components. For example, after T cell receptors (TCRs) are engaged by antigens, TCRs clusters containing cholesterol and Lck are formed (Janes et al., 1999). It is evident that upon stimuli, certain microdomains can be observed by light microscopy. But the origin of these visible microdomains is still yet to be elucidated. That is, whether the microdomains are formed from smaller lipid rafts or there are no such smaller lipid rafts existing on the surface of resting cells is still unclear. Furthermore, recent studies have shown that the co-fraction of putative lipid raft components in detergent-resistant membrane (DRM) might be artifacts induced by the detergent treatment.

Therefore, to understand the microstructure of the cell membrane, it is critical to develop more sensitive and less perturbing methods than present biochemical approaches. Fluorescence recovery after photobleaching (FRAP) has been used to measure the average diffusion coefficient of specific surface molecules labeled with fluorophores on the cell membrane. It was found that some surface molecules are more confined on the cell membrane than on the artificial membrane. Most of the putative lipid raft components belong to such category, suggesting there are some diffusion barriers on the cell membrane keeping these molecules from diffusing freely as on the artificial lipid bilayers. Fluorescence correlation spectroscopy has also been used to identify different

diffusional mobilities belonging to raft markers and non-raft markers on the cell membrane (Bacia et al., 2004). Foster resonance energy transfer (FRET) has also been employed to study the spatial relationships between surface molecules labeled by acceptor and donor fluorophores (Kenworthy et al., 2000; Rao and Mayor, 2005; Sharma et al., 2004), and generated mixed results about the existence of lipid rafts on the resting cell membrane. Single particle tracking (SPT) has been used in our lab to characterize the heterogeneity of the cell membrane. In SPT, surface molecules are labeled with nano-sized particles and their lateral motions on the cell membrane are recorded by tracking the particles bound to the surface molecules. It has been found that there are small regions on the cell membrane in which surface molecules are temporarily confined with lower diffusion rates, indicating the biophysical heterogeneity of the cell membrane. These regions are called transient confinement zones (TCZs). TCZs can be detected even on relatively unstimulated cells, though with less abundance.

On the other hand, the relationship of TCZs and lipid rafts defined in the original lipid raft model is still to be defined. To further exploit the advantages provided by SPT, which are minimal perturbation, long observation period and dynamic recording, we used SPT to investigate the lateral motion of clustered surface molecules. The clusters being investigated were induced by deliberate cross-linking and were of a size less than 150 molecules. Clusters of this size are still beyond the resolution of optical microscopes and represent the population formed immediately upon ligation/cross-linking events before they coalesce into bigger patches, usually at the order of more than 1000 molecules, which are visible under

microscopes. In this work, we found that in addition to TCZs, such cross-linking induced clusters also demonstrated another unique behavior, transient anchorage, where the gold-labeled clusters stopped moving for up to 10 seconds. The occurrence of transient anchorage suggests the involvement of other factors than thermal forces and surface heterogeneity. In the following experiments, transient anchorage was characterized, and the possible mechanisms were discussed and evaluated using SPT. It is concluded that transient anchorage requires the involvement of Src family kinases, cholesterol, caveolin. Interpreting results from the experiments, it is speculated that transmembrane proteins, cytoplasmic adaptor proteins and cytoskeleton also participate in transient anchorage. A preliminary model has been developed to include the findings of this study and to serve as the working hypothesis for uncovering the molecular mechanisms behind transient anchorage.

Chapter 3: Methods to measure the lateral diffusion of membrane lipids and proteins

In this chapter, methods are discussed to measure lateral mobility of membrane lipids and proteins using techniques based on the light microscope. These methods typically sample lateral mobility in very small, micron-sized regions of the membrane so that they can be used to measure diffusion in regions of single cells. The methods are based on fluorescence from the molecules of interest or from light scattered from particles attached to single or small groups of membrane lipids or proteins. Fluorescence recovery after photobleaching (FRAP), fluorescence correlation spectroscopy (FCS) and Single particle tracking (SPT) are presented in that order. FRAP and FCS methodologies are described for a dedicated wide field microscope although many confocal microscopes now have software permitting these measurements to be made; nevertheless, the principles of the measurement are the same for a wide field or confocal microscope. SPT can be applied to trace the movements of single fluorescent molecules in membranes but this aspect will not be treated in detail.

1. Fluorescence recovery after photobleaching (FRAP)

Fluorescence recovery after photobleaching (FRAP) is a single cell technique used to study the mobility of fluorescent molecules. The method has been employed since the mid 1970s to examine molecular mobility in the plasma membrane, other organellar membranes and the cytoplasm (Kapitza et al., 1985). A resurgence in use occurred in the 90s due to the advent of GFP fusion proteins (Lippincott-Schwartz et al., 2001).

In a FRAP experiment, a pulse of high intensity light from a laser is used to photobleach fluorophores, typically in a small micron-sized region. Subsequently, fluorescence recovers due to lateral transport of unbleached fluorophores into the bleached region and concomitant movement of bleached fluorophores out of the region. Under optimal conditions, the recovery kinetics depend only on the molecular mobility, which usually is determined by the diffusion and flow of the labeled molecules as well as the binding kinetics of the fluorescent molecules to anchored or slowly moving structures. In most cases, a diffusion coefficient and/or flow velocity and mobile fraction can be determined.

The simplest version of the photobleaching technique is spot photobleaching which is schematically depicted in Fig. 1. First, the emission, $F(t < 0)$, produced by fluorophores in a small region of interest on the membrane is measured. Second, an intense, short photobleaching pulse is applied to the same region of the specimen, rapidly destroying a substantial amount of fluorescence in that region. Right after this photobleaching pulse, the fluorescence $F(0)$ in the same region is measured again and this is defined as time zero. The recovery of the fluorescence within the

photobleached area is recorded as a function of time with a beam coincident with the photobleaching beam and of the same intensity as that used to measure F ($t < 0$). The recovery curve increases in fluorescence intensity from F (0) at time zero to F (∞) at the time when the recovery is considered complete.

The kinetics of recovery can be empirically characterized by the time, $\tau_{1/2}$, required to reach 50% of complete recovery. The mobile fraction is calculated by the extent to which the initial fluorescence F ($t < 0$) is regained by the end of the experiment

$$\text{Mobile Fraction} = \frac{F(\infty) - F(0)}{F(t < 0) - F(0)} \quad (1)$$

Fluorophores immobile on the time scale of measurement are indicated by mobile fractions of less than 100%. In calculating transport coefficients, it is assumed that spontaneous recovery of fluorescence does not occur and the probe beam does not itself induce photobleaching. If recovery occurs by lateral diffusion, the diffusion coefficient, D, is given by

$$D = \frac{r_o^2 \gamma}{4\tau_{1/2}} \quad (2)$$

where r_o is the $1/e^2$ radius of the Gaussian profile laser beam used for both photobleaching and measuring fluorescences, and γ is a parameter that depends on the extent of photobleaching, varying slowly from 1.0 to about 1.2.

1.1. Instrumentation

FRAP measurements require three major components: (1) a laser, operating in the TEM_{00} mode which produces a Gaussian intensity profile, that serves as the excitation source for both photobleaching and measurement of fluorescences; (2) a microscope equipped for epifluorescence; and, (3) a detector for the fluorescence emission combined with electronics to record the measured fluorescence intensity. Fig. 2 shows a schematic diagram for the optical and electronic elements in a FRAP system such as described above. A beam divider and recombiner (Koppel, 1979) is placed in the light path between the light source and the microscope. This device, consisting of two optical flats placed at +45° to the optical axis, divides the laser beam into two beams and then after an arbitrary distance recombines them on the optical axis. One beam serves as a high power bleaching beam, and the other is for measuring the fluorescence by exciting the specimen with low power. A shutter is placed after the first optical flat in the path of the high power beam to block it during the time of recovery. This shutter only opens during the photobleaching step, which generally takes one hundred milliseconds or less. Mechanical shutters that can open and close in a few milliseconds are recommended (e.g. Uniblitz, NY). Another second optical flat is positioned after the shutter at −45° in order to merge the two beams back into one that travels along the optical axis of the microscope. Mirrors usually are required to direct the laser beam along the optical axis into the epi-port of the microscope. Focussing the laser beam on the specimen by the objective depends on the lenses in the microscope that are before the objective in the excitation path. In the simplest case of no lenses, the beam is brought to focus by a simple

convex lens (Kusumi) on the primary image plane in the excitation path. In this case, the beam radius on the specimen plane is approximately that on the primary image plane divided by the magnification of the objective. The specimen is therefore excited or bleached by the laser in a very small area that is determined primarily by the power of the objective.

The fluorescence emitted from the specimen is detected with a cooled photomultiplier (PMT) placed on or near an image plane of the microscope. Cooling can reduce the noise by 100-fold when the temperature drops from room temperature to −25 °C. Water-cooled thermoelectric elements are preferable to fan-driven air-cooling because the fan vibrations will be transmitted through the microscope. To avoid physical damage caused by exposing the PMT to fluorescence excited by the bleaching beam, another shutter blocks the PMT only when the specimen is being bleached. The signal, a photocurrent, from the PMT is amplified and passed to a computer for analog to digital conversion if required and recorded by a multichannel, multiscaling card. A photon counting photomultiplier is used and pulses from the PMT are counted on a multiscaling analyzer card in the computer. Often a pinhole is placed on the image plane just before the PMT—this serves to eliminate out-of-focus fluorescence, much as in a confocal microscope (Koppel, 1979). A computer is also employed to control the entire FRAP experiment. The investigator can set the timing of the opening and closing of the shutters, control the length of data collection period or make other optional commands for the system, such as background noise collection and the length of each sampling period.

Laser beam size calibration is critical for the FRAP set-up, since the calculation of diffusion coefficients (see Eq. (2)) depends on the square of the laser beam size. A preliminary estimate can be obtained by estimating the size of the fluorescent spot excited by the focused laser beam using an ocular micrometer. A suitable test specimen can consist of fluorophores dissolved in an aqueous solution which is sandwiched between a microscopic coverslip and a slide. The weaker laser beam used for measuring is focused to the median plane between two glass/water interfaces. The rapid diffusion of fluorophores in water and the low excitation intensity of the measuring beam markedly reduces apparent bleaching and will keep the fluorescence profiles about the same level during the calibration. An alternative way to image the laser beam for diameter measurements is to use an immobile dil film. Two hundred microliters of a 1 mg/ml dil solution is mixed in amyl acetate on the slide and let stand for 8 s; the slide is placed for another 30 min in a covered jar containing amyl acetate solution at the bottom to produce a saturated vapor. Finally, the slide is allowed to dry and a coverslip is placed on top of the dil deposited region. The final thickness of the dil film is <1 μm. For the quantitative purposes, a series of images is taken with a linear detector such as a CCD camera. The diameter of a beam with a rectangular intensity profile is easily measured because of the contrast between the dark background and fluorescent region. For the more usual case of Gaussian beam profile, an intensity line scan through the image of beam is performed using the image analysis software. The 1/e2 radius can be read off this scan as the point where the intensity drops to 13.5% of its peak value. Orthogonal scans characterize asymmetries in the beam intensity profiles.

1.2. Analysis of recovery curves

A number of procedures have been developed to extract diffusion coefficient from fluorescence recovery curves (Elson and Qian, 1989; Koppel et al., 1976; Petersen and Elson, 1986; Soumpasis, 1983). Axelrod et al. (Koppel et al., 1976) have developed spot photobleaching analysis procedures that can be applied to both Gaussian and uniform laser beam profiles. For the Gaussian profile bleaching and measuring beam, a simple three-point fitting is used and this gives quite a good estimate of D. The initial fluorescence, F ($t < 0$), the fluorescence immediately after photobleaching, F (0), and the maximum recovered fluorescence, F (∞), are measured. If one knows the mechanism of lateral transport, i.e., diffusion or flow, then from the measured half-time of recovery, the diffusion coefficient and/or flow velocity can be determined using Eq. (2). For these calculations to be correct, two experimental constraints must be observed. First, the bleach time, τB, should be $<1/10\ \tau 1/2$. Second, the ratio of the fluorescence immediately after bleach to that before bleach should be >20%. These restraints insure that the initial condition imposed by the bleach is preserved as required by the theory. There are several software programs to extract two diffusing components from a recovery curve. For example, Gordon et al. (Gordon et al., 1995) have developed a fitting procedure that is able to calculate both one- and two-component diffusion parameters with maximal accuracy by employing a statistical computation. The procedure is specifically designed to analyze the recovery curves in the presence of significant noise due to low signal levels, which is common in FRAP studies of cell membranes. F-tests are performed to compare the goodness of the fit between the one- and two-component fit.

This allows one to determine if it is justified statistically to employ an additional component to fit the data. Fitting to more than two components is difficult unless the recovery curves have a high signal to noise ratio.

2. Fluorescence correlation spectroscopy (FCS)

Fluorescence correlation spectroscopy (FCS) is another technique which can be used to study translational mobilities in membranes. Similar to FRAP, this method requires molecules of interest to either be fluorescent or, alternatively, be conjugated to a fluorescent dye or protein. In this method, the fluctuations in the fluorescence intensity from a minute sample observation volume are recorded and temporally autocorrelated to reveal information about the concentration and dynamics of the fluorescent species in the sample (Fig. 3). Recent technological advances have revived FCS as a useful technique for measuring translational mobilities in solution including in the cytoplasm and nucleus as well as in cellular membranes. FCS has been the subject of many recent reviews (Bacia and Schwille, 2003; Elson, 2004; Haustein and Schwille, 2004; Hess and Webb, 2002; Levin and Carson, 2004; Thompson et al., 2002) and a book (Rigler and Elson, 2001).

The instrumental set-up for FCS is very similar to that required for FRAP with the major exceptions typically being the addition of a hardware correlator but no high intensity photobleaching light beam (Fig. 2). There are many procedural differences though. To start, because the measured signal in an FCS experiment constitutes fluctuations from the time averaged fluorescence intensity, the lower the absolute number of molecules in the sample volume the greater the measured signal. This is accomplished by

defining a very small observation volume and by analyzing very dilute samples such that only very few molecules are present in the observation volume at any one time. The sample observation volume is in most cases defined by focusing a laser to a diffraction-limited spot in the sample plane. The observation volume is further limited by placement of a pinhole in an image plane in front of the detector which essentially limits collection of emitted photons to those emanating from the specimen plane. Alternatively, FCS has also been used with total internal reflection fluorescence excitation in conjunction with a pinhole (Lieto et al., 2003) or by two photon excitations (Berland et al., 1995) and (Schwille et al., 1999a). Commercial versions are available from Carl Zeiss (ConfoCor2, www.zeiss.com), Leica (FCS2, www.leica.com) and ISS (Alba, www.iss.com).

The theoretical framework of FCS was originally described in the early 1970s (Magde, ; Magde et al., 1974; Schwille et al., 1999a). The normalized fluorescence fluctuation autocorrelation function is given by

$$G(\tau) = \frac{\langle \delta F(t) \delta F(t+\tau) \rangle}{\langle F \rangle^2} \qquad (3)$$

where δF(t) is the difference between the instantaneous fluorescence at time t and the time average of the fluorescence intensity, left angle bracketFright-pointing angle bracket,

$$\delta F(t) = F(t) - \langle F \rangle \qquad (4)$$

and τ is the correlation time. Numerous forms of the autocorrelation function have been derived to account for a variety of experimental conditions. In general these forms are dependent on the shape of the observation volume, the detection efficiency and on the properties of the studied fluorophore.

In the case of a free diffusion in three dimensions and with a Gaussian observation volume, the temporal autocorrelation function G(τ) is given by

$$G(\tau) = \frac{1}{N}\left(1 + \frac{\tau}{\tau_{1/2}}\right)^{-1}\left(1 + \left(\frac{r_o}{z_o}\right)^2 \frac{\tau}{\tau_{1/2}}\right)^{-1/2} \quad (5)$$

where N is the number of fluorescent molecules in the observation volume, τ1/2 is the characteristic diffusion time and is a measure of the average time it takes a fluorescent molecule to diffuse through the observation volume, and ro and zo are the radial and axial distances where the laser intensity of the observation volume has decayed to $1/e^2$. In the case of diffusion within a membrane (diffusion in two dimensions; limit as zo → 0), the autocorrelation function G(τ) is given by

$$G(\tau) = \frac{1}{N}\left(1 + \frac{\tau}{\tau_{1/2}}\right)^{-1} + c \quad (6)$$

where c is a constant that has been added to correct for the slow fluorescence fluctuations that are commonly experienced in membranes. In either case, the

diffusion coefficient, D, of the fluorescent molecule is calculated from the characteristic diffusion time, τ1/2

$$D = \frac{r_o^2}{4\tau_{1/2}} \quad (7)$$

where the distances ro and zo are obtained by careful independent calibration of the sample observation volume with a fluorescent dye of known solution diffusion coefficient (i.e., Rhodamine-6-G; D = 280 μm2/s). Autocorrelation functions for a fast and a slowly diffusing species are given in Fig. 3B. It is also possible to calculate the concentration of fluorescent molecules in the sample, C] from

$$[C] = \frac{N}{N_A V} = \frac{1}{G(0) N_A V} \quad (8)$$

where NA is Avogadro's number and V is the sample observation volume which for a typical Gaussian confocal volume is given by

$$V = 2\pi r_o^2 z_o \quad (9)$$

In general, FCS can measure diffusion coefficients over five orders of magnitude ranging from diffusion of small molecules in solution (similar300 μm2/s) to the diffusion of membrane proteins within cell membranes (similar0.01 μm2/s) (Axelrod et al.) and where slow diffusion measurements are typically limited by photobleaching of the fluorescent molecule as it moves

through the observation volume. To date, FCS has been used to measure diffusion of fluorescent lipids and proteins in model membranes including giant unilamellar vesicle (GUV) membranes (Bacia et al., 2004; Kahya et al., 2003; Kahya et al., 2004; Korlach et al., 1999; Schwille et al., 1999a; Schwille et al., 1999b) and in cellular plasma membranes (Bose et al., 2004; Hegener et al., 2004; Schwille et al., 1999a) as well as diffusion of fluorescent molecules within the cytoplasm (Hegener et al., 2004; Schwille et al., 1999a; Watanabe et al., 2004) and the nucleus (Politz et al., 1998; Watanabe et al., 2004).

Potential problems with using FCS for measuring translational mobilities within a cell membrane include the difficulty associated with aligning the observation volume to coincide with the membrane. Another problem is that the depth of the observation volume (not, vert, similarμm) is significantly larger than the thickness of biological membranes (not, vert, similar10 nm) which can lead to mixed sampling of the mobility in the membrane and adjacent aqueous surrounds. This problem can be avoided by selecting probes with high membrane specificity or probes whose quantum yield is significantly larger when located in the hydrophobic interior of the membrane as opposed to adjacent aqueous surround. Problems with aligning the observation volume to coincide with a membrane have been addressed in some commercial instruments by combining FCS with confocal microscopy. Using this set-up one may first align and image a particular membrane by confocal microscopy and subsequently switch to FCS. Cellular autofluorescence can also be a problem when studying translational mobility in cells. This problem is best addressed by selecting fluorescent dyes or

proteins that emit in the red part of the spectra (i.e., DsRed, Cy5). For a more thorough discussion of these limitations and others see the reviews by Schwille and co-workers (Bacia and Schwille, 2003) and Webb and co-workers (Hess and Webb, 2002) and the recent book on FCS (Rigler and Elson, 2001).

3. Single particle tracking (SPT)

Single particle tracking (SPT) is a powerful method for studying the movement of individual or small groups of proteins or lipids in the plasma membrane of live cells or in model membranes. The dynamic behavior of these molecules can be recorded and then analyzed to reveal the microstructure of the plasma membrane. By attaching antibody-coated sub-micron colloidal gold particles to molecules on the cell membrane, intense Rayleigh scattering can be detected from particles as small as 30 nm in diameter. While 30 nm is too small to resolve in the light microscope, the scattering pattern appears at the diffraction limit of not, vert, similar250 nm and the position of the centroid of the pattern can be measured to not, vert, similar10 nm precision. This property of gold particle SPT permits researchers to explore the structure of membranes on nanometer length scales and on ms or smaller time scales. SPT using gold particles has an important advantage in that the signal does not photobleach thereby extending the observation time; however, the 30 nm or 40-nm diameter gold particles may produce unwanted perturbations of structures. The time resolution of SPT depends on the frame rate of the camera being used. Video cameras using the NTSC standard have a sampling frequency of 30 frames/s, while those using the

PAL standard have a frame rate of 25 Hz. However, SPT has been performed with specialized video cameras that have time resolution of 25 μs (Fujiwara et al., 2002). The SPT experiment is depicted schematically in Fig. 4.

3.1. Methodology

To make gold particles traceable markers for membrane molecules, they are coated with antibodies or ligands that can either directly or indirectly bind to the target surface molecules. Conjugation of gold to antibodies requires care and has been described in several publications (Fujiwara et al., 2002; Politz et al., 1998; Simson et al., 1998). In addition to gold particles that users themselves conjugate to antibodies or ligands, there are now several commercial ready-to use options, such as gold particles covalently coated with anti-biotin, anti-mouse IgG antibodies, streptavidin and protein A (BBInternational Ltd., Britain). In the case of indirect binding between gold particles and surface molecules, cells are first incubated with primary antibodies that specifically recognize the target molecules on the cell membrane, and after washing out the excess primary antibodies, gold particles coated with appropriate agents are applied to the cells. After excess non-bound gold particles are removed by washing, cells are mounted on a slide and sealed with wax. In this way, the sample can be observed using an inverted microscope oil condenser to provide maximum resolution in the image.

In a typical SPT system, a video camera is connected to an optical microscope. Video signals (analog) from the camera are transmitted to a recording device, for example, a VCR or a computer equipped with a frame grabber video card and hard drives of appropriate capacity.

Single gold particles can be imaged in bright field by employing analog and digital contrast enhancement (Lee et al., 1998; Simson et al., 1998). In our version, a bright field 100X oil immersion objective (NA 1.3) and an oil-immersion condenser (NA 1.4) are employed. The images are further magnified by a factor of four (total magnification of 400X) and projected to a Hamamatsu Newvicon camera (Bridgewater, NJ). After background subtraction and contrast enhancement by image processing software (Image-1, Universal Imaging, West Chester, PA), the processed video images are displayed on the monitor and recorded by a recording device (such as the computer hard drive, DVD disc or video tape) in real time. Video enhanced differential interference contrast microscopy (DIC) can also be used to image gold particles (Gelles et al., 1988).

If SPT movies are recorded in analog format (such as on video tape), the conversion of the movies to digital format is required before the data can be analyzed. The choice of tracking software is important to faithfully track a single particle without mistaking it for other particles or even the cellular structures that give images similar to gold particles. Due to the surface topography and/or stage drift, a single particle can go out of the focal plane and then may or may not come back. The consequence of the gold particles going out of focus, combined with background brightness fluctuations due to the nature of cells, is that the gold particles might not retain the same image characteristics throughout the whole trajectory. The tracking software has to be flexible enough to consistently track a single gold particle when its shape and contrast changes from time to time, yet be powerful enough to distinguish the particle of interest from other seemingly similar entities during the tracking

process. In addition, the tracking software should be able to fit the image of the shape of the gold particles with a kernel of choice and find the centroid of the particle with sub-pixel precision. To choose appropriate tracking software, careful tests using sample movies of single particles moving under various conditions, including the presence of multiple particles, or in fields with dark spots as part of the background, are required. Nevertheless, even the best tracking software does not always work in certain situations. Therefore it is essential to have a manual track function built in the software, letting the user instruct the program where to find the single particle with a cursor.

For most SPT experiments, it is common to have more than 1000 frames in a single movie file, which usually exceeds 700 Mb. Therefore it is important for the computer to have both fast processing speed and large data storage capacity.

3.2. Rudimentary analysis of trajectories

A schematic of how lateral diffusion coefficients can be calculated from a single particle trajectory is given in Fig. 5a. The x-y coordinates of single particles in each frame of the movie are located by the selected tracking software. After converting the trajectories in the movies into lists of x- and y-positions in time, the displacements are calculated for each time interval, Δt. As one can see, there are fewer data points as the time interval grows so the uncertainty at long time intervals is correspondingly greater (Qian et al., 1991). The displacements are squared and averaged to give the mean square displacement (MSD). MSD is related to the lateral diffusion coefficient by the formula,

$$\mathrm{MSD} = \langle r^2 \rangle = 4D\Delta t \quad (10)$$

However, one of the most interesting and revealing aspects of SPT is the analysis of departures from random diffusion. For example, such analyses have yielded confined diffusion of particles on various time scales (Dietrich et al., 2002; Fujiwara et al., 2002; Simson et al., 1995), anomalous diffusion (for review, see (Saxton and Jacobson, 1997)) or directed flow of particles (Sheetz et al., 1989) (figure 5b). The relationship between confined diffusion and membrane structure and function has been interpreted in terms of nanoscale structures in and adjacent to the plasma membrane and remains a controversial area that is under active investigation.

Chapter 4: Hardware and software engineering for lateral diffusion measurement-- Configuration of the FRAP system

Introduction

As mentioned in Chapter 2, FRAP measurements with a wide field microscope require three major components: (1) a laser, operating in the TEM_{00} mode which either produces a Gaussian intensity profile, or with a pinhole, a circular intensity profile, that serves as the excitation source for both photobleaching and measurement of fluorescences; (2) a microscope equipped for epifluorescence; and, (3) a detector for the fluorescence emission combined with electronics to record the measured fluorescence intensity. A pair of shutters (shutter 1 and 2 in figure 2) is placed to control the passage of light during the FRAP process: shutter 1 is placed between the beam divider and combine; shutter 2 is placed in front of the PMT. The timing of the opening/closing of the shutters is very important in order to protect the PMT from overexposure due to the overloading of photons while photobleaching and collect critical initial recovery data at the moment immediately after photobleaching. After the data collection, the photon counts of the FRAP course are analyzed with a curve fitting program to estimate the diffusion coefficient and the mobile fraction of the fluorescent species in interest. In this chapter, the hardware programming of the shutter and the curve fitting algorithm are described. In addition, this chapter also includes

the algorithm for the detection of transient confinement zones out of the trajectories recorded in single particle tracking experiments.

FRAP

Hardware

The mechanical shutters controlling the passing of the laser beam were purchased from Uniblitz. The control board (BNC 2120) was purchased from National Instruments. The beam splitters were purchased from Newport. The multiscalar card which is connected to the PMT was purchased from MSC cooperation . The PC which conveys the electric commands to the control card is a PC installed with Windows 98 operating system. The control board is connected to the PC, the mechanical shutters, and the multiscalar card.

Timing program

The Visual basic module for the National Instruments control board was also purchased from National Instruments. The module was used to program the timing of sequential operations during FRAP. The algorithm for the timing program is listed below:

(1) Once the start button of the FRAP program is hit by the user on the computer screen, a TTL signal is sent to trigger the multiscalar card to start counting the input intensity. The shutter blocking the bleaching laser beam placed in the middle of BDC is now set at the closed position (figure 2), thus the bleaching beam cannot pass through sample. The shutter placed before PMT is set at the open position so that multiscalar card is reading the fluorescent intensity as F0.

(2) When the timer reaches the time set to start the photobleaching, the control board sends a signal to open the shutter after beam splitter to allow the bleaching laser beam to pass through and bleach the fluorophores in the sample. Simultaneously the shutter before PMT is set closed to protect PMT from damage caused by overexposure. Therefore no fluorescence readout is available during the bleaching period.

(3) After the photobleaching is completed, the control board resets the shutters: the shutter after the beam splitter is closed again and the shutter before the PMT opens again. The recovery of the fluorescence is now being recorded with the user-specified sampling rate.

(4) When signal collection is finished (the length of such period is set by users), the control board sends another TTL signal to the multiscalar card to stop the recording and start transferring the data to the PC from the built-in memory of the multiscalar card. The data will be stored as a 2-column text file, with the first column being time points and the second one being the fluorescence intensity (amplified by the PMT).

Data Fitting

We adopted the method published previously by Gordon et al. (Gordon et al., 1995). The fitting procedure is based on Marquardt algorithm to calculate both one- and two-component diffusion parameters with maximal accuracy by employing a statistical computation. The program is written in Matlab programming language. The FRAP model is described below:

(1) The prebleach intensity is defined as Fi, F(O) being the first postbleach intensity, and K being given by Eq. 1

$$F(0) = F_i[1 - \exp(-K)]/K. \quad \text{(Eq. 1)}$$

K is a measure of the fractional depth of bleach, F(O)/Fi.

(2) The one-component model takes the form

$$F(t) = \phi F_i f(t) + (1 - \phi)F(0) \quad \text{(Eq. 2)}$$

where F(t) is the intensity at time t, Φ represents the mobile fraction (), and f(t)is the series

$$f(t) = \sum_{n=0}^{\infty} \left[\frac{(-K)^{-n}}{n!}\right]\left(1 + n + \frac{2nt}{\tau}\right)^{-1} \quad \text{(Eq. 3)}$$

where T is the characteristic time of diffusion.

(3) To form the two-component model, two one-component recovery curves are added together. The subscripts 1 and 2 distinguish the two diffusing components with a common K value. The model is based on the two series

$$f_1(t) = \sum_{n=0}^{\infty} \left[\frac{(-K)^{-n}}{n!}\right]\left(1 + n + \frac{2nt}{\tau_1}\right)^{-1} \quad \text{(Eq. 4)}$$

and

$$f_2(t) = \sum_{n=0}^{\infty} \left[\frac{(-K)^{-n}}{n!}\right]\left(1 + n + \frac{2nt}{\tau_2}\right)^{-1} \quad \text{(Eq. 5)}$$

(4) Now the two-component model then becomes

$$F(t) = \alpha[\phi_1 F_i f_1(t) + (1 - \phi_1)\, F(0)] + (1 - \alpha)[\phi_2 F_i f_2(t) + (1 - \phi_2)F(0)] \quad \text{(Eq. 6)}$$

where α is the fraction of component 1. This model has six parameters: K, τ1, τ2, α, Φl, and Φ2. However, three of the parameters, α, Φ1, and Φ2, are dependent, meaning that their values cannot be determined uniquely. Even

though the six-parameter model works well, the five-parameter model below performs better at lower signal levels and, thus, the five-parameter model was used to produce the results in the present report. Substituting Eq. 1 for F(O) in Eq. 6 and rearranging yields

$$F(t) = F_i\{\alpha\phi_1 f_1(t) + (1-\alpha)\phi_2 f_2(t) + [1 - (\alpha\phi_1 + (1-\alpha)\phi_2)][(1 - \exp(-K))/K]\} \quad \text{(Eq. 7)}$$

(5) In Equation 7 the three parameters α, Φ1, andΦ2 occur only as the products amp and (1 - α)Φ2, indicating that they are dependent. The two products are used in place of the three original parameters, which yields two independent parameters (αΦ) and (1 - α)Φ2) for a total of five parameters. The two products are the mobile fractions weighted by the component fractions (weighted mobile fractions). It is not possible to determine uniquely either the mobile fractions or the component fraction, but only the weighted mobile fractions. The fraction of the fluorescence due to immobile molecules of both components (net or aggregate immobile fraction), before the bleach is 1 - (αΦ1 + (1 -α)Φ2).

The curve fitting algorithm is listed below:

(1) Perform a three-point fit (Axelrod et al., 1976) that estimates the half-time of recovery, the depth of bleach parameter (K), and the mobile fraction () assuming one diffusing component. The three-point fit method measures three intensity values relative to the baseline (dark noise): the prebleach intensity (Fi), the intensity immediately after the bleach (F(O)), and the intensity at the last part of the recovery curve, which is assumed to be at complete recovery (Axelrod et al., 1976).

(2) Smooth the recovery curve (optional). A smoothed point is created by taking a contiguous group of points in the raw recovery curve and replacing the group with a single point usually derived by averaging the group or interpolating within the group. The smoothing algorithm reported by Petersen et al. (Petersen et al., 1986) is modified. In the beginning, only one raw data point is counted as a group until reaching the first postbleach point, after which the group size is increased by two points. The group size keeps increasing by points after every 2 groups of data points are processed. This strategy allows sampling the fast early rising part of the curve best and smoothes the late, slow rising part the most.

(3) Use the three-point fit estimates as the starting guesses for a one-component fit, which assumes the one-component model above (Eq. 2). The results of the one-component fit are recorded and also used to generat starting guesses for the two component fit, which assumes the two-component model above (Eq. 7). For both models the number of terms of the series (Eq. 3 for the one-component model or Eqs. 4 and 5 for the two-component model) increased with the estimated value of K as in the report by Petersen et al. (Petersen et al., 1986). The numbers of points of the recovery curve to be analyzed are varied by the user. The results of the analysis program are the fitted parameters, the reduced X^2 values for the one- and two-component fits, and the F-test values comparing the two fits. The fit with higher F-test value is selected as the model better fitted the FRAP curve.

Single Particle Tracking

TCZ detection program (rewritten in Matlab)

In order to perform batch analysis, the TCZ detection program was redesigned to enable the selection of multiple files before analysis starts. In the new program, the result for each file selected is stored in the specified directory. Furthermore, a spreadsheet listing the statistics of the analysis results is also generated and saved.

The algorithm for TCZ detection used in this new program is the same as the previously described one, which was developed by Simson et al. (Simson et al., 1995) (also see the details in Chapter 4).

Evaluating centroid detection algorithm for particle tracking purpose

In work with Shawn Janiro, a Biomedical Engineering graduate student of master degree, whom I supervised, we evaluated the available programs for dynamic centroid detection used to the trajectory of mobile particles. The programs under investigation include video spot tracker (created by Dr. Russel Taylor from Computer Science Department at University of North Carolina), Labview NI vision component (National Instruments, Texas), Metamorph (Universal Imaging), and IDL (RSI, Colorado). Accuracy, efficiency, user-friendliness, and module-based functionality expansion are evaluated for each program. And it is determined that IDL v 6.3 has the best overall performance. IDL can detect the centroid of a moving particle, whose trajectory is known, with less than 3% error rate even in a noisy and fluctuating background. In addition, IDL provides capacity to build on the basic tracking routine for future more specific use. Users can track objects by keying commands or using a pre-compiled graphic user interface.

Chapter 5: Transient confinement zones: a type of lipid raft?

Many important signaling events are initiated at the cell membrane. To facilitate efficient signal transduction upon stimulation, membrane microdomains, also known as lipid rafts, are postulated to serve as platforms to recruit components involved in the signaling complex, but few methods exist to study rafts in vivo. Single particle tracking provides an approach to study the plasma membrane of living cells on the nanoscale. The trajectories of single gold particles bound to membrane proteins and lipids are characterized in terms of both random and confined diffusion; the latter occurs in “transient confinement zones”. Here we review transient confinement zones and some of their implications for membrane structure and function.

Introduction

In the Singer-Nicolson fluid mosaic model, the cell membrane is considered as a 2-D oriented solution of integral proteins in a viscous phospholipid bilayer (Singer and Nicolson, 1972). However, more recent single particle tracking (SPT) experiments suggest the need to modify the original model (Jacobson et al., 1995). In addition, over the past decade, numerous biochemical studies have demonstrated that a significant fraction of plasma membrane lipids including cholesterol, saturated phospholipids, and sphingolipids exhibit some degree of detergent resistance. This fraction also

includes glycosylphosphatidylinositol (GPI)-anchored proteins and certain transmembrane proteins (Brown and London, 1997; Brown and London, 1998; Brown and Rose, 1992). Although detergent-resistant membranes (DRM) are postulated to represent putative submicron-sized lipid rafts on the cell surface (for reviews, see(Jacobson and Dietrich, 1999; Kusumi et al., 2004; Simons and Ikonen, 1997; Simons and Ikonen, 2000; Simons and Toomre, 2000)), the in vivo correlate of DRM has not been established. In detergent extraction experiments, the lipid and protein compositions of DRM depend strongly on the nature and concentration of the nonionic detergent used, as well as the time and the temperature of the extraction (Schuck et al., 2003; Shogomori and Brown, 2003). Moreover, it has been observed that the nonionic detergent Triton-X can promote formation of microdomains in model membranes(Heerklotz, 2002).

Therefore, assuming DRM are lipid rafts could provide a grossly misleading view of membrane microstructure. Different approaches other than detergent extraction are required to test the lipid raft hypothesis.
Usually, light microscopy resolution is limited to ~250 nm, meaning that microdomains smaller than this cannot be measured, although they can be detected if they are bright enough. By fluorescence microscopy, many raft components, as defined by detergent extraction, appear uniformly distributed although there are notable exceptions (Malinska et al., 2003); but clustering can be seen by fluorescence resonance energy transfer in some cases (Sharma et al., 2004; Zacharias et al., 2002).

SPT provides an alternative way to investigate the heterogeneity of cell membranes. By attaching antibody-coated submicron- sized colloidal gold

particles to molecules on the cell membrane, the dynamics of a small number of molecules or even a single molecule can be recorded and studied by tracing trajectories of the particles. SPT has two advantages: (i) The particles used give a signal that does not photobleach, thereby extending the observation time; and (ii), 40-nm gold particles are small enough to reduce the chance for perturbation. Available detection methods are based on the intense Rayleigh scattering, which can be applied to submicron particles down to 30 nm in diameter. Although SPT presents insights about membrane structures, it does have limitations. The path of single particles is not controllable, and SPT only covers a small area of the cell membrane. Also, when coating specific antibodies on the gold particles, it is very difficult to achieve precise valence control, meaning that more than one surface molecule may anchor the particle to the cell membrane. Rather than being exclusively 2-D random walks, the trajectories of single particles that are attached to surface molecules on the cell membrane often exhibit a variety of trajectories in addition to random walks. These include directed movement, confined movement, and anchored behavior (Fig. 6) (Simson et al., 1995; Simson et al., 1998), a result not explicitly anticipated by the Singer-Nicolson fluid mosaic model. Temporary confinements (Fig. 6B) are detected in the trajectories of membrane proteins that cannot be accounted for by the large family of random walks (Simson et al., 1995). These temporary confinements are termed transient confinement zones (TCZ). The existence of TCZ supplies another piece of evidence supporting membrane lateral heterogeneity, although the mechanism of transient confinement remains to be elucidated.

Detection of TCZ and the significance

When the lateral mobility of surface molecules on the cell membrane is examined by SPT, careful analysis is required to characterize the molecular trajectories. To be able to distinguish confined diffusion or directed transport, both of which reveal interesting biological features, from simple Brownian motion, it is necessary to establish algorithms that can justifyably reject those random walks that might look confined or directed.

Saxton (Saxton, 1993) has studied the 2-D diffusion in a series of Monte Carlo simulations. For 2-D random walkers, the probability j that a molecule, having diffusion coefficient D, will stay in a region of radius R, for a period of time t is given as

$$\log \varphi = 0.2048 - \frac{2.5117\,Dt}{R^2} \qquad (1)$$

This allowed Simson et al. (17) to develop an algorithm that detects confinements due to nonrandom means. Simson et al. introduced the probability level index L to characterize the probabilities of nonrandom confinements. The relationship between

L and f is:

$$L = \begin{cases} -\log(\varphi) - 1 & \varphi \le 0.1 \\ 0 & \varphi > 0.1 \end{cases} \qquad (2)$$

The higher the value of L is, the more likely a particle is confined due to a nonrandom mechanism. Because a random walk can temporarily mimic confinement, the goal of this algorithm is to reject those random walks that look like transient confinement.

To achieve this goal, the algorithm takes advantage of the fact that the peaks of probability profiles arising from mimicked confinement in random walks are usually lower and narrower than genuine ones. By experimenting

with both actual and simulated data, an optimized threshold (Lc) value is obtained so that the algorithm is able to detect real confinement with a minimal error rate less than 0.07% and to reject mimicked ones with an accuracy of about 98.5%. Simson's algorithm also implements a low pass filter to smooth the probability profile (Simson et al., 1995), thereby suppressing short-lived mimicked confinement from Brownian motion. After applying the algorithm to SPT trajectories, TCZ are detected, and the sizes and dwell time of particles in the TCZ are computed. The computed sizes of confinements and dwell time of particles in TCZ are dependent on the time resolution of SPT. That is because with greater time resolution, two different confinements that are very close are more likely to be distinguished. At lower time resolution, such a structure will appear as a single bigger confinement with a longer dwell time. For this reason, before comparing transient confinement analysis results in terms of size and dwell time, it is important ensure the data were acquired at similar time resolution.

Example of TCZ

Previous papers from our group have reported TCZ being detected by SPT for GPI-anchored proteins, glycosphingolipids (GSL), and phospholipids (Dietrich et al., 2002; Sheets et al., 1997; Simson et al., 1995; Simson et al., 1998). These TCZ are of a size ranging from 100 to 300 nm in diameter, and the diffusing particles are trapped for several seconds. Moreover, upon the suppression of GSL synthesis (Sheets et al., 1997) or depletion of cholesterol (Dietrich et al., 2002), the abundance and the size of the zones were markedly diminished. Dietrich et al. (Dietrich et al., 2002) also found that TCZ

could be revisited after particles escaped, suggesting that zones could be stable for tens of seconds and that diffusion within the zones was reduced by a factor of ~2, which was consistent with the particle diffusing within in a cholesterol-rich, liquid-ordered state. These experiments indicate that TCZ exhibit some of the physical and chemical characteristics postulated for hypothetical lipid rafts.

A few other examples of confinement have appeared in the literature. Daumas et al. (Daumas et al., 2003a; Daumas et al., 2003b) have studied the diffusion of a G-protein-coupled receptor, the μ-opioid receptor, by gold particle SPT. In their experiments, they observed transient confinement as well. However, they fitted the data to a different mathematical model, in which the diffusing surface proteins are confined to a domain which itself diffuses, the confinement being due to “long-range attraction between membrane proteins.”

In other words, the surface proteins belong to a “walking confined diffusion mode” composed of long-term random diffusion of a domain characterized by $D = 1.3 \times 10^{-3}$ μm2/s and short-term confined diffusion within the domain characterized by $D \sim 10^{-1}$ μm2/s.

SPT has been applied to the study of the kinetics of membrane-bound receptors as well. Instead of gold particles, Meier and colleagues (Meier et al., 2001)used 0.5 μm latex beads to track the movement of gephyrin, a ligand for glycine receptor, by SPT. They observed that particles attached to glycine receptor subunits expressed without gephyrin moved rapidly in the plane of the membrane for most of the time, with an estimated diffusion coefficient of $\sim 2.7 \times 10^{-2}$ μm2/s, whereas co-expression of glycine receptors that contain the gephyrin binding domain and gephyrin-green fluorescent protein (GFP)

resulted in long periods of confinement characterized by very limited slow movement interspersed with periods of rapid particle movement. The transient confinements were spatially associated with gephyrin- GFP clusters visualized by fluorescence microscopy. And diffusion coefficients of particles during confined periods were 1–1.5 orders of magnitude lower than those measured during rapidly moving periods. Based on these observations, Meier and colleagues (Meier et al., 2001) speculated that limited diffusion of receptors during the confined state may be due to slow diffusion of the entire gephyrin cluster with bound receptors.

Transient confinement is induced by cross-linking

Fine details of membrane lateral diffusion. A continuing puzzle is why diffusion coefficients of membrane lipids are reduced by a factor of 5–20 from those on artificial bilayers (Jacobson et al., 1987; Lee et al., 1993; Ritchie et al., 2003; Sonnleitner et al., 1999; Subczynski and Kusumi, 2003). To address the problem, Fujiwara et al. (Fujiwara et al., 2002; Murase et al., 2004b) measured the movement of 1,2-dioleoyl-sn-glycero-3-phosphoethanolamine (DOPE), which by virtue of its two unsaturated acyl chains, is considered to be a typical nonraft lipid. By using SPT with an ultra-high temporal resolution of 25 μs per frame, as opposed to the conventional video sampling rate of 33 ms per frame, they found that the cell membrane is compartmentalized with regard to translational diffusion of DOPE. That is,a single DOPE molecule is temporarily confined within a 30 to 230-nm compartment, the size depending on cell type (Murase et al., 2004b). for several milliseconds on average before it hops to a neighboring compartment.

This compartmentalization is dependent on the actin-based cytoskeleton underneath the cell membrane but is not sensitive to the removal of extracellular matrix or cholesterol.

To explain their results, they proposed a membrane picket fence model (Fig. 7) (Fujiwara et al., 2002; Ritchie et al., 2003). In the model, both lipids and proteins, regardless of their raft association, exhibit free diffusion at rates comparable to those on artificial membranes within plasma membrane compartments that are delimited by immobilized transmembrane proteins as anchored-pickets linked to the subjacent membrane cytoskeleton. The occasional hop to an adjacent compartment, which occurs roughly once every 11 ms, rate-limits the long-range diffusion. However, even if the effect from hop diffusion is taken into account, it does not completely explain the smaller long-range diffusion coefficients of GPI-anchored proteins such as Thy1 measured by SPT at 33 ms time resolution (Dietrich et al., 2002). The implication is that aggregation of proteins and/or lipids is the major reason for the reduced motion of surface molecules, primarily because the gold particles are pauci-valent. Indeed, it is plausible to regard the TCZ as a membrane domain that attracts certain crosslinked entities and thereby transiently confines these surface complexes.

Cleavage of antibodies that recognize the specific surface proteins into single-valence fragments (Fabs), followed by careful titration, permits coating gold particles in an apparent one-to-one ratio with these Fabs or ligands to surface proteins, making the particle effectively monovalent. Gold particles that recognize CD59, another GPI-anchored protein, exhibit similar diffusion rates and hop intervals when compared to DOPE at 25-us resolution.

Moreover, under these apparently monovalent conditions, no TCZ were observed at 33-ms resolution (Kusumi et al., 2004; Subczynski and Kusumi, 2003). By contrast, when the gold particles were deliberately made multivalent by coating the particles with intact antibodies at high concentration, short-range CD59 diffusion was considerably slower and TCZ were detected at 33-ms time resolution (Kusumi et al., 2004; Subczynski and Kusumi, 2003). This suggests that some form of cross-linking is required to observe TCZ. Interestingly, cross-linking-induced TCZ required cholesterol, intact actin filaments, and Src family kinase (SFK) activity. Intracellular calcium signals were closely associated in time with the formation of the TCZ. Taking all their data together, the Kusumi group (Ritchie et al., 2003) now suggests that lipid rafts are so small and short-lived in resting cells (Fig. 7) that a non-cross-linked single raft protein has almost the same short-range diffusion coefficient as a nonraft lipid molecule.

However, upon cross-linking, the molecular cluster caused by multivalent gold particles not only diffuses more slowly but also triggers processes that stabilize lipid rafts. These cross-linked complexes are termed “cluster rafts.” Cluster rafts are formed by various cross-linking agents including antibodies, and they are more stable and may be bigger than lipid rafts in resting cells. The cluster raft-stabilizing process is speculated to be caused by transient tethering onto the actin-based membrane skeleton. The likely involvement of signaling molecules in stabilizing cluster rafts suggests that lipid rafts serve as platforms that could locally initiate signal transduction (Simons and Ikonen, 2000).

To examine and verify the model proposed by Kusumi group (Ritchie et al., 2003), our laboratory now is investigating the behavior of other GPI-anchored proteins by SPT. To achieve maximal cross-linking, we incubated C3H fibroblast cells first with biotinylated anti-Thy1 antibodies, then anti-biotin antibodycoated

colloidal gold particles, after which anti-mouse IgG antibodies were added (Fig. 8). We observed that maximal cross-linking increased the percentage of time (the relative confinement time, RCT) that a single particle spends in TCZ by more than twofold compared with control treatments without anti-mouse IgG applied. Under these conditions, we observed repeated transient anchorage, which means, in our experiments, that the displacement range of the particles is within ~20 nm for several seconds before the gold particles resume their trajectories on the cell membrane. The transient anchorage observed in maximal cross-linking experiments is distinct from conventional transient confinement. Whereas in normal transient confinement gold particles are localized in an area ranging from 100 to 300 nm in diameter, in which the particles move with a reduced diffusion coefficient, transient anchorage apparently stops the gold particles (to <20 nm). Addition of SFK inhibitor 4-amino-5-(4-chlorophenyl)-7-(*t*butyl) pyrazolo(3,4-d) pyrimidine (PP2) reversed the RCT increase owing to transient anchorage, indicating SFK play a role in cross-linking-dependent TCZ formation/stabilization.

Cholesterol depletion further reduced the RCT to 2%, indicating that cholesterol is essential for both TCZ existence and transient anchorage. Another GPI-anchored protein, CD73, a 5 -ectonucleotidase, exhibited qualitatively similar behavior in IMR-90 human fibroblasts, suggesting that

these crosslinking-induced effects are quite general. In summary, confined behavior can be broken into two classes: true in-plane transient confinement and transient anchorage (SFK-mediated) of cluster rafts, as depicted in Figure 9. It appears that SPT can be used to reveal details of the early steps in crosslinking- induced signal transduction.

Chapter 6: Mechanisms of transiently anchoring cross-linked glycosyl-phosphatidylinositol-anchored proteins to the membrane associated cytoskeleton -- Signal transduction via membrane nanodomains

How outer leaflet plasma membrane components, including glycosyl-phosphatidylinositol-anchored proteins (GPIAPs), transmit signals to the cell interior is an open question in membrane biology. By deliberately cross-linking several GPIAPs under antibody conjugated 40-nm gold particles, transient anchorage of the gold-particle induced clusters of both Thy-1 and CD73, a 5' exonucleotidase, occurred for periods ranging from 300 ms to 10 seconds in fibroblasts. Transient anchorage was abolished by cholesterol depletion, the addition of the Src family kinase inhibitor, PP2, or in Src-yes-fyn knockout cells. Caveolin-1 knockout cells exhibited reduced transient anchorage time, suggesting the partial participation of caveolin-1. By contrast, a transmembrane protein, the cystic fibrosis transmembrane conductance regulator (CFTR), exhibited transient anchorage that occurred without deliberately enhanced cross-linking; moreover, it was only slightly inhibited by cholesterol depletion or SFK inhibition and depended completely on interaction of its PDZ binding domain with the cytoskeletal adaptor, EBP50. We propose that cross-linked GPIAPs become transiently anchored via a

cholesterol dependent, SFK-regulatable linkage between a transmembrane cluster sensor and the cytoskeleton.

Introduction

The general signaling mechanisms by which cross-linking of membrane determinants induces linkage to the cytoskeleton is a long standing issue dating back to the original patching and capping observations (Raff et al., 1970) and the ideas of Singer (Holifield et al., 1990; Singer, 1977). More recently such attachments have assumed clearer physiological and pathological importance. For example, receptor-induced dimerization (Lidke et al., 2005) causes retrograde transport off the filopodia to distal sites for further processing. Bead induced clustering of integrins and CAMs causes retrograde transport of these molecules away from the leading edge and considerable effort has been devoted to the manner by which different sized ligand-coated beads induce clusters of cell adhesion molecules to link to the retrograde actin flow (Felsenfeld et al., 1996; Suter et al., 1998; Suter and Forscher, 2001). Viral particles, after binding to membrane receptors, are eventually associated with the cytoskeleton in different ways (Ewers et al., 2005; Pelkmans et al., 2002). T cell activation, initiated by ligation, is mediated by TCR-containing microclusters that reorganize in an actin-dependent manner (Yokosuka et al., 2005).

Even lipids and glycosylphosphatidylinositol-anchored proteins (GPIAPs), when cross-linked, undergo patching and capping (Schroit and Pagano, 1981; Holifield et al, 1990); and GPIAPs can signal across the plasma membrane. Binding of antibody to a number of GPIAPs was shown

early on to induce an association with Src family kinases (SFKs) (Stefanova et al, 1991). Cross-linking the GPIAP, Thy-1, on T lymphocytes results in mitogenesis. (Kroczek et al., 1986; Zhang et al., 1992). Group B coxsackieviruses start the process of infection of epithelial cells by binding to and then clustering the GPIAP co-receptor, decay-accelerating factor (DAF), on the apical surface (Coyne and Bergelson, 2006). Transmembrane signaling has been speculated to occur in nanodomains such as lipid rafts when clusters are induced via receptor ligation and cross-linking (Simons and Toomre, 2000) and such signaling may serve to link the cluster to the cytoskeleton (Kusumi et al., 2004). But the precise mechanisms of how GPIAPs signal and link to the cytoskeleton remain to be elucidated. This issue remains central in the study of the functionality of membrane microdomains (Kusumi et al, 2004).

In this study, we use a novel feature of single particle tracking (SPT) trajectories as an assay to begin a dissection of how linkage of certain GPIAP and transmembrane proteins to the membrane associated cytoskeleton may be regulated. SPT has been used to study membrane heterogeneity on various time and distance scales. Using video rate SPT, gold particles bound to membrane lipids and proteins were found temporarily corralled in transient confinement zones (TCZs) (Chen et al., 2004; Dietrich et al., 2002; Sheets et al., 1997; Simson et al., 1995). With much higher time resolution, gold particles bound to lipids and glycosyl-phosphatidylinositol (GPI)-anchored proteins undergo compartmentalized “hop diffusion” on the millisecond time scale (Kusumi et al., 2005). Most previous experiments were aimed at producing pauci- or univalent gold in order to minimize the number of

membrane molecules bound to gold so as to minimize artifacts due to cross-linking membrane molecules (Murase et al., 2004a). By contrast, in this study, we deliberately used the gold particle to form clusters of GPI-anchored proteins, mimicking the clusters formed under physiological conditions. The size of clusters associated with gold particles is much smaller than the size of clusters which were seen by immunostaining in previous studies (i. e. patches), which may represent on the order of 1000 molecules (Holifield et al., 1990). This protocol produced a unique nanoscale signature in the SPT trajectories, termed transient anchorage, that depends on Src family kinases (SFKs), PI3 kinase, cholesterol and caveolin-I. In some respects, our study confirms and extends the unpublished studies of Suzuki et al. (Suzuki et al., 2002) using the GPI-anchored protein, CD59. A transmembrane protein, the cystic fibrosis transmembrane conductance regulator (CFTR), also exhibits transient anchorage that strictly depends on its C-terminus PDZ binding domain but it is regulated differently than the GPIAP anchorage.

Results

Transient Anchorage

Mild cross-linking of membrane molecules by pauci-valent gold is most likely the reason for transient confinement (Kusumi et al., 2004; Murase et al., 2004a). However, in our hands, this type of transient confinement was not sensitive to inhibitors of Src family kinases (data not shown) in contrast to results reported by Kusumi and co-workers (Kusumi et al, 2004). We reasoned that perhaps our level of cross-linking was insufficient to induce involvement of SFKs. Therefore, we employed three different layers of cross-

linking antibodies (figure 11a), in order to collect the GPI-anchored proteins of interest together under and proximate to a single gold particle. The trajectories of these clusters on the cell membrane reveal how signal transduction influences the lateral motion of GPI-anchored proteins that are sufficiently cross-linked.

We chose to investigate two GPI-anchored proteins, Thy-1 and CD73, a 5' exonucleotidase, both endogenously expressed. The trajectories of both molecules exhibited a surprising feature: a significant number of temporary anchorage events could be observed in the video record (figure 11b and supplemental movie 1). To automatically identify the transient anchorage, a detection program was developed. Transient anchorage, in which particles stop (no displacement within experimental error) transiently, is distinguished from transient confinement in which single particles still diffuse but in a slower and confined manner (Dietrich et al., 2002). The periods of transient anchorage varied from several hundred milliseconds to more than ten seconds as shown in an example from cross-linked CD73 on IMR 90 cells and are bimodally distributed (figure 11c). The longer anchorage times are directly visible in the video record. Figure 12a shows how the total relative confinement, combining both transient confinement zones and transient anchorage for both Thy-1 (top) and CD73 (bottom), was increased by the maximal cross-linking protocol up to seven times compared to the control (leftmost) in which the tertiary cross-linking antibody was not applied. Note that, despite different definitions of transient anchorage and transient confinement, sometimes transient anchorage points overlapped with TCZs. Therefore, in order to avoid overestimation of RCT+RAT, the time segments

in the trajectory in which transient anchorage was detected were removed and the trajectory concatenated. This operation resulted in decreased relative confinement time in trajectories in which transient anchorage was detected. Transient anchorage only occurred after the addition of the tertiary antibodies (figure1 a, bottom right) and showed titration behavior (table 1) so that there was an optimum at a dilution of ~ 1:100 with the final concentration of 20 ug/ml. The dependence of transient anchorage on the concentration of tertiary antibody suggests that a critical size and/or number of cross-linked GPI-anchored proteins is required for transient anchorage (Harder and Simons, 1999). Having too many tertiary antibodies will result in a competition for the available binding sites offered by the primary antibodies; this will lead to monovalent binding of the tertiary antibody with diminished cross-linking and transient anchorage.

Transient anchorage also occurs with preassembled complexes: estimate of cluster size

The number of molecules cross-linked in one cluster is important for constructing a detailed mechanism of transient anchorage. In the maximal cross-linking protocol, primary antibodies are first bound to specific GPI-anchored proteins (figure 11); anti-biotin gold is then added decorating the surface at very low concentration. Finally tertiary antibody is added. Under these conditions, it is difficult to estimate the size of the cluster aggregated under one particle. In addition, the possibility of distal patches of cross-linked GPI-anchored proteins globally affecting the behavior of the gold particles cannot be excluded.

Therefore, we pre-assembled gold particle-antibody complexes to test whether transient anchorage would still occur. These complexes contain anti-biotin gold with biotinylated anti-mouse-IgG antibodies and anti-Thy-1 antibodies. An approximation to the number of primary antibodies bound to each gold particle in the pre-assembled complexes was made by estimating the contact area between the gold particle and cell membrane (see Supplemental Methods). The estimate suggests that the maximal number of gold-bound Thy-1 molecules is likely to be less than 135 and probably much less. These pre-assembled complexes exhibited transient anchorage, although the relative anchorage time was somewhat reduced (20%) compared to the original protocol (28%) (Figure S2b). The bi-modal distribution of anchorage times was similar to that seen in the maximal cross-linking SPT experiments (Figure 11d). Thus, a cluster of less than 135 GPIAPs is sufficient to induce transient anchorage.

Regulation of transient anchorage

Role of cholesterol: To examine the role of cholesterol, which is found enriched in detergent-resistant membranes (DRMs) and is hypothesized to be an essential component of rafts, in transient anchorage, we performed cholesterol depletion prior to the maximal cross-linking. SPT trajectories obtained from treated cells were compared with control. Transient anchorage was not detected in cells depleted of cholesterol by MβCD (Thy-1 and CD73; figure 12a, top and bottom, respectively) or removed by cholesterol oxidase (CD73) (figure 12a, bottom panel). Both Thy-1 and CD73 showed reduced

transient confinement upon cholesterol depletion consistent with previous studies (Dietrich et al., 2001; Sheets et al., 1997).

Role of Src family kinases: GPI-anchored proteins, such as CD59 and Thy-1, are found to couple with SFKs which are distributed in the inner leaflet of the cell membrane, in order to effect signal transduction (Stefanova et al., 1991). It has also been shown that filamentous actin accumulates under patches of GPI-anchored proteins (Harder and Simons, 1999). The actin enrichment requires activities of Fyn and Lck kinases (Harder and Simons, 1999), both of which belong to the Src family. A plausible hypothesis is that SFKs mediate the process of tethering the cross-linked GPI-anchored protein clusters to the membrane associated cytoskeleton. Indeed, a form of transient confinement with the GPI-anchored protein, CD59, has been shown to be mediated by Lck (Kusumi, 2004). Hence, we treated cells with the specific SFK inhibitor, PP2, prior to the cross-linking. Transient anchorage was completely suppressed for both GPI-anchored proteins tested (figure 12a), indicating SFKs are critical for the stabilization of the clusters. Transient confinement, however, was not significantly affected. Since transient anchorage occurs with pre-assembled particles, the possibility that global activation of SFKs by the maximal cross-linking protocol is responsible for transient anchorage is excluded.

We used the Src, Yes and Fyn triple knock-out mouse fibroblast (SYF) cells to confirm these results. Our anti-human CD73 antibody bound to CD73 on SYF cells and Src rescued SYF cells as assessed by immunostaining (data not shown) and western blots from these cells (figure 12b). SYF defective cells showed no transient anchorage and reduced confinement

similar to PP2 treated cells. But transient anchorage was restored in Src-rescued SYF cells (figure 12c). Thus SFK activity is crucial for the transient anchorage phenotype.

Role of PI3 Kinase: Phosphoinositides PIP2 and PIP3 co-patch with cross-linked raft components (Janes et al., 1999). It has also been shown that signaling via cross-linked GPIAP and choleratoxin-labeled cholesterol-containing clusters on the cell surface is blocked by both tyrosine kinase and PI3 kinase inhibition (Krauss and Altevogt, 1999), suggesting involvement of PIP_2 and PIP_3 in signaling events induced by cross-linking. In addition, PIP2 and PIP3 found in inner leaflet microdomains are also involved in cytoskeletal regulation (Janmey and Lindberg, 2004). These findings suggest that changing the balance of PIP_2 and PIP_3 by inhibiting PI3K might affect transient anchorage. To test this possibility, prior to SPT experiments, IMR 90 cells were incubated with the PI3 kinase inhibitor, LY294004, for 15 minutes. Compared to control cells, PI3 kinase-inhibited cells exhibited over 3- fold greater transient anchorage (figure 13a). But the proportion of the longer anchorage times was drastically reduced (compare figure 13b to figure 11c). Moreover, inspection revealed that half of the trajectories (23/47) exhibited bi-directional movements in the PI3 kinase inhibited cells with excursions up to several μm (figure 13c).

Role of Caveolin: Since cholesterol depletion also disrupts the structure of caveolae, which has been demonstrated by electron microscopy (Dreja et al., 2002; Parpal et al., 2001), a plausible possibility was that caveolae and caveolin might have a role in transient anchorage. Supporting this possibility, patches of cross-linked GPIAPs were found associated with caveolae (Mayor

et al., 1994). By co-immunostaining of caveolin-1 and maximally cross-linked Thy-1 on C3H cells, we confirmed that cross-linked GPI-anchored Thy-1 partially co-localizes with caveolin-1(figure 14c,d). Similar results were obtained for CD73 and Caveolin-1 in IMR-90 cells (figure 14a, b). By contrast, if cells were prefixed and subjected to maximal cross-linking, minimal colocalization was observed (data not shown).To test the involvement of caveolin I in the transient anchorage phenotype, we used Caveolin-1 knockout mouse embryonic fibroblasts. The expression of Caveolin-1 was checked in knockout and control wild type embryonic fibroblasts by immunostaining and confirmed the absence of Caveolin-1 on the cell surface of the knockout cells but not the wildtype (data not shown). Also, both caveolin-1 wt cells and knockout cells express CD73 (Figure 12b). As shown in figure 14c, the RAT was reduced from about 45% in wildtype cells to about 15% on Caveolin-1 knockout cells. After PP2 treatment to inhibit SFKs, the RAT was reduced to less than 5% in both knockout and wildtype cells. A similar effect was observed when cholesterol depleted from both cell types. The result suggests that Caveolin-1 contributes to the transient anchorage significantly, although apparently other mechanisms are also involved, as indicated by the persistence of transient anchorage that is PP2 inhibitable in caveolin-1 knockout cells.

Transient anchorage exhibited by a transmembrane protein is regulated in a different manner

To further test if the critical role of SFKs in transient anchorage of GPI-anchored proteins is related to phosphorylation-enabled cytoskeletal association of clustered GPI-anchored proteins, we examined the diffusion

behavior of a transmembrane protein, the cystic fibrosis transmembrane conductance regulator (CFTR). The C-terminal cytoplasmic domain of CFTR associates with the actin cytoskeleton via NHERF PDZ proteins (EBP50 and E3KARP) and ezrin (Raghuram et al., 2003; Short et al., 1998; Sun et al., 2000). If transient cytoskeletal association is the cause of transient anchorage, and cross-linking is necessary to recruit SFKs for clustered GPI-anchored proteins to be linked to the cytoskeleton, then CFTR might be expected to demonstrate transient anchorage in a cross-linking and SFK-independent manner. Furthermore, if the requirement for cholesterol in the transient anchorage of GPI-anchored proteins is because SFKs can only be recruited under the clusters through cholesterol-mediated nano-domains, then CFTR might also be expected to demonstrate transient anchorage independent of cholesterol.

CFTR tagged with an extracellular HA-epitope was expressed in C3H cells and labeled with biotinylated anti-HA antibodies and anti-biotin antibody conjugated gold. We found that CFTR displayed transient anchorage in the absence of tertiary cross-linking antibody (Figure 15). Upon PP2 or cholesterol depletion treatment, gold-conjugated HA-CFTR demonstrated only a modest reduction in relative anchorage time (Figure 15), whereas both Thy-1 and CD73 showed a marked decrement in relative anchorage time after the same treatments (figure 12a). Also, deletion of the PDZ binding domain in CFTR, the delta 4 mutant, (Gentzsch et al., 2004), caused transient anchorage to be almost completely eliminated (Figure 15) indicating that NHERF(EBP50) PDZ proteins and ezrin provide the key linkage to the cytoskeleton required for transient anchorage of CFTR to occur. Thus,

GPIAPs exhibit a much more marked dependence of transient anchorage on SFK and cholesterol than does transmembrane CFTR. This suggests a mechanism by which cross-linked GPI-anchored proteins could exploit, via a cholesterol-mediated nanodomain followed by SFK regulation, the normal linkages of transmembrane proteins to the cytoskeleton (see Discussion).

Discussion

Robust transient anchorage was observed with the maximal cross-linking protocol. The pre-assembled complexes clustering 135 or fewer Thy-1 GPI-anchored proteins are shown to be sufficient to trigger transient anchorage comparable to the clusters formed by maximal cross-linking. Cholesterol is essential for gold particle-bound clusters to be transiently anchored on the cell surface, suggesting that a cholesterol-dependent nanodomain is formed under maximally cross-linked gold particles. The cross-linking triggered signaling events involve SFK cascades, PI3 kinase and caveolin I. What molecular mechanisms might account for this phenomenon? The broad outlines of how different modes of transient anchorage might occur can be gleaned from recent reviews. Simons and Toomre (2000) suggested that cross-linking of receptors might be a key to effecting signal transduction by either altering partitioning into existing raft domains or bringing smaller rafts together. Kusumi et al (2004) suggested that one mode of coupling clustered GPIAPs may involve an unspecified transmembrane protein and recruitment of small inner leaflet rafts containing lipid linked signaling molecules to the site of the “cluster raft” on the outer leaflet.

To focus future experiments, we propose a somewhat more specific working hypothesis (Figure 16) using these ideas as a starting point. In this model, cross-linking induces cholesterol dependent nanodomains ("cluster rafts") to form on both inner and outer-leaflet. Such clusters would include key transmembrane proteins bridging the inner and outer leaflets, so that signals could be transmitted across the membrane in discrete locations. These proteins would be included from the outset and/or incorporated after collision of the cluster with the transmembrane protein. Whether initial anchoring is assisted by "oligomerization-induced trapping" (Kusumi et al, 2005) is an open issue. When an activated SFK randomly partitions into such a nanodomain on the inner leaflet, phosphorylation by SFK induces a resident transmembrane molecule to attach to the actin cytoskeleton through adaptor proteins. The attachment results in a transient anchorage event that continues until the SFK is deactivated and a recruited phosphatase dephosphorylates the resident linking molecule.

Specific molecular players can be accommodated by this generic hypothesis. A novel SFK substrate, Csk binding protein (Cbp or PAG), was identified recently as a transmembrane protein binding partner for Csk, a kinase which regulates SFKs by phosphorylation at their C-terminal regulatory site (Matsuoka et al., 2004). There is also evidence indicating Thy-1 is associated with Cbp (Durrheim et al., 2001). Furthermore, after phosphorylation by proximate SFKs, Cbp binds the ERM binding protein (EBP50) via its PDZ domain and thus associates with the cytoskeleton through ERM proteins (Itoh et al., 2002). Thus, Cbp is a plausible candidate for the transmembrane protein component of the hypothesis. Indeed, we have

obtained results which are at least consistent with transient anchorage of GPIAPs proceeding via the EBP50-ERM-actin cytoskeleton linkage: An EBP50 binding transmembrane protein, CFTR, exhibits transient anchorage without employing the maximal cross-linking protocol and removal of the C-terminal PDZ binding domain of CFTR, which binds EBP50, in the delta 4 mutant abrogates transient anchorage (Figure 15). Our hypothesis therefore suggests that there is a common mode of cytoskeletal binding for both CFTR and GPIAPs (via EBP50:ezrin), but two different ways to couple to these adaptors, either directly (CFTR) or indirectly (GPIAP) via the formation of nanodomains and SFK regulation. Indeed, a regulatable ezrin linkage to Cbp was recently hypothesized to link rafts containing the B cell receptor to the lymphocyte cytoskeleton (Gupta et al., in press). That is, a common mode of cytoskeletal binding (via EBP50: ezrin), but two different ways to couple to these adaptors, either directly (CFTR) or indirectly via the formation of microdomains.

Although not explicitly included in the model discussed above, the fact that Caveolin-1 is partially involved in transient anchorage and associates with the F-actin cross-linking protein, filamin (Stahlhut and van Deurs, 2000), suggests another possible mode of transient anchorage that would involve caveolae. In their studies of the mobility of Simian Virus 40 (SV40) on the cell surface prior to and just after its entry into the cell, the Helenius group also found a partial dependence on Caveolin 1 (Damm et al., 2005). Their findings can be compared and contrasted to our study. After diffusing, SV40 often stops, as opposed to being transiently anchored, as a prelude to internalization via cavolin-1 dependent or independent pathways. However,

only the caveolin-1 independent internalization pathway of SV40 requires tyrosine kinase activity and cholesterol. In our work, transient anchorage does not exclusively depend on caveolin-1, suggesting at least two pathways to anchorage, but both pathways depended on cholesterol and SFK. The Helenius group also used SPT to study the diffusion behavior of murine polyoma virus–like particles (VLPs)--which are 45 nm in diameter and similar to the size of gold particles--bound to live cell membranes and found cholesterol-dependent but SFK-independent confinement (Ewers et al., 2005). VLPs exhibited confined diffusion in small zones 30-60nm in diameter that differs from transient anchorage in the fact that neither SFKs, nor Caveolin are required for confinement. Confinement requires cross-linking of viral receptor (ganglioside) which promotes linkage to the actin cytoskeleton in an as yet undefined way. In general, it could be anticipated, based on extensive study of viral interactions with the cell membrane, that multiple modes of transient anchorage would exist (Marsh and Helenius, 2006).

Unexpectedly, inhibition of the conversion of PIP2 into PIP3 by PI3 kinase enhances transient anchorage and induces directional motion in a significant fraction of trajectories. It is possible that PIP2 may preferentially partition into the inner-leaflet microdomains induced by the cross-linked clusters of GPI-anchored proteins, and transient anchorage might then be formed via PIP2, to adaptor proteins that are associated with the actin cytoskeleton underneath the cell membrane, such as the ERM family proteins (Fievet et al., 2004). The bi-directional movements observed in some of the trajectories suggests that PIP2 clusters that participate in transient anchorage might also bind to motor proteins through their FERM or PH domains, thus

contributing to the directed transport of cross-linked clusters by walking along cytoskeletal filaments. Binding between clustered PIP2 and motor proteins also provides a possible explanation for the disappearance of longer stopping periods, since the motor proteins are active most of the time and might be expected to move the cluster directionally with short pauses (Kural et al., 2005).

Taken together, our data suggests the transient anchorage phenotype may be regulated in different ways depending on the biological context. Moreover, the transient anchorage assay presented here should be valuable in defining precise linkages to the cytoskeleton and how they are regulated.

Materials and Methods

Cells

C3H 10T1/2 murine fibroblasts (American Type Culture Collection, Rockville, MD) and IMR 90 human fibroblasts were maintained in BME and DMEM, respectively, both supplemented with 10% fetal bovine serum, 100 units/ml penicillin, and 100 µg/ml streptomycin. 2 to 4 days before an SPT experiment, fibroblasts were plated onto sterile 22 mm × 22 mm coverslips (#1.5, glass) that were placed into 35-mm Petri dishes at an appropriate cell density that yielded single cells for SPT measurements. Cells were depleted of cholesterol by treatment with 5 mM MβCD (Sigma, St. Louis, MO)at 37°C for 30 minutes in unsupplemented medium or with 0.5 units of cholesterol oxidase (C8273, Sigma) at 37°C for 1 hour in complete medium, respectively. Src -/-, Yes -/-, Fyn -/- mouse embryonic cell line (SYF) (ATCC, MD) and the SYF cell line with restored c-Src expression by the retroviral vector pLXSH

(SYF+) (ATCC, MD) were used to examine the effect of Src family kinases on transient anchorage. The Caveolin-1 deficient mouse embryonic cell line (Cav-1 -/-) and its wildtype parental cell line, which were a generous gift from Dr. Martin Schwartz, were used for experiments investigating the role Caveolin-1 in transient anchorage. HA-tagged CFTR protein was expressed in C3H cells by lipofectamine transfection.

Gold conjugation to cells

Procedure I: Anti-biotin mouse IgG gold (BBInternational, UK) was dissolved in HAMS F12 nutrition mixture (Life Technologies/Gibco-BRL) supplemented with 25 mM HEPES and 15% serum (HHS), sedimented by centrifugation for 15 min at 11,000 × *g* at 4°C and resuspended in HHS. Cells on the cover slips were first incubated with biotinylated primary antibodies (monoclonal mouse anti-Thy-1 antibody clone 19EX5, 1.5 mg/ml or monoclonal mouse anti-human CD73 antibody clone AD2, a gift from Dr. Linda Thompson, 0.15 mg/ml) for 10 minutes, then washed for 3 times with 1 ml of HH. Then the coverslip was mounted to form an open chamber on the slide with spacers on two parallel edges of the coverslip. 100 µl of the solution containing anti-biotin gold (4.5 x 10^9 particles/ml) was injected into the chamber and incubated with cells for 10 minutes at 37°C. Unbound gold particles were removed by washing with 100 µl of HH (HHS without serum). 100µl of the solution containing tertiary antibodies (goat anti-mouse IgG from Zymed, California, 0.02 mg/ml) for the purpose of maximal cross-linking was injected into the chamber at this time if required. A final washing step with 100-µl-injected HHS was performed to remove unbound gold. For SPT of CFTR, biotinylated mouse anti-HA antibody (clone 16B12, 0.1 mg/ml from

Covance, New Jersy, USA) was used as the primary antibody, followed by the addition of anti-biotin gold. SPT was then performed without addition of cross-linking tertiary antibodies. For all experiments, after the gold particle incubations, the sample chamber was sealed with wax and mounted on the microscope; particle trajectories were recorded for the following 30 minutes at 37°C, maintained by an air curtain incubator.

Procedure II (Pre-assembled complexes): Gold particles conjugated with antibodies specific to GPI-anchored proteins of interest were assembled before addition to the cells. Pre-assembled complexes (figure S2a) were made by mixing 20 µl of anti-biotin gold (4.5 x 10^{11}particles/ml), 2 µl of biotinylated goat anti-mouse IgG antibodies (2mg/ml) and 20 µl of mouse anti-Thy-1 antibodies (15.5 mg/ml) in HHS solution with a final volume of 2 ml. The pre-assembled complexes then were spun down, resuspended, and added to the cell membrane for SPT experiments as described above for Procedure I. On the basis of the number of anti-biotin conjugated to gold (150 antibodies/particle) as specified by the manufacturer (BBInternational, UK), biotinylated goat-anti-mouse IgG antibodies (2.6 x 10^{-11} mole) added were in 10 fold excess over the anti–biotin antibodies coated on gold, and mouse anti-Thy-1 antibodies (10^{-9} mole) added were in 40 fold excess over the goat anti-mouse IgG antibodies.

Immunofluorescence

Colocalization of cross-linked GPIAPs with caveolin I: Cross-linking of GPIAPs was accomplished by incubating cells with biotinylated primary monoclonal antibodies followed by anti-biotin gold (BBInternational, UK) and Alexa 488 polyclonal goat anti-mouse IgG antibody (Molecular Probes,

Oregon) as in procedure I in “Gold conjugation to cells”. Cells were fixed with a mixture of 2% paraformaldehyde and 2.5% glutaraldehyde for 10 minutes, washed for 3 times with PBS, and permeablized with 1% NP-40. Rabbit anti-mouse Caveolin-1 antibody (Santa Cruz, CA) and Texas Red-labeled goat anti-rabbit IgG antibody (Oncogene Research, UK) were used to stain the Caveolin-1 inside the cell. Following extensive washing in PBS, cells were observed using an Olympus IX-81 fluorescence microscope with a X100 objective. As a negative control in immunostaining, cells were pre-fixed in the 2% paraformaldehyde-2.5% glutaraldehyde mixture after which the maximal cross-linking protocol was employed; under such conditions, clustering of the GPIAPs would not be expected.

Time lapse gold imaging for SPT

Computer-enhanced video microscopy, described earlier (Lee et al., 1991), was used to image colloidal gold bound the plasma membrane of fibroblast cells. Briefly, the cell lamella with bound gold was imaged in brightfield mode and recorded with a video camera (Newvicon Hamamatsu). After real-time background subtraction and contrast enhancement with an image processing unit (Argus 20, Hamamatsu, Japan), video frames were recorded in time lapse mode (1800 frames with 30 frames/s) on the hard disk of a computer (O2, Silicon Graphics, Mountain View, CA). Recorded movies were analyzed by the commercial software package ISEE (Inovision Corp., Durham, NC) that identifies relative changes of gold particle positions on the cell lamella with a precision of ±20 nm. All trajectories were visually inspected to ensure correct tracking of gold particles.

Data Analysis

Trajectories of gold particles obtained from SPT movies were analyzed for both transient confinement and transient anchorage. The detection for transient confinement zones (TCZs) was done as before (Simson et al., 1995). Transient anchorage detection software was designed to detect regions of trajectories where no displacement within experimental error occurred—as defined by all aspects of measurement stability. By recording movies of gold particles firmly glued on coverslips using nail polish and then detecting particle centroids over the time recorded, it was determined that 95% of centroids fell within +/-25 nm along both x and y axis (figure S1). A program was developed to recognize fragments from a trajectory as transient anchorage events when the displacement in successive frames was less than 25 nm in both the x and y dimensions. Note that transient anchorage differs from immobilization in which the particle does not move during the experimental observation time of a particular cell. To further characterize transient anchorage, we defined the relative anchorage time (RAT) as:

Sum of durations in which a single particle is transiently anchored*/*total time of trajectory

To avoid over-estimation of total confinement, given that transient anchorage sometimes overlaps with TCZs, transient anchorage segments were removed from the trajectories, and the remaining trajectory fragments were concatenated before TCZ detection.

Estimation of maximum number of GPIAPs bound to pre-assembled complexes

We made this estimate using the following considerations. Gold particles almost appear to float on the membrane and can diffuse rapidly. This suggests that they are not nearly enveloped by the plasma membrane. The degree to which they can bend the membrane around them will determine the maximum number of membrane antigens the pre-assembled complex can bind. The bending modulus determines how facilely the membrane can be molded. However, the bending modulus will depend on the length scale examined. For example, if the particle is over an actin or spectrin filament, bending will not be as easy as if the particle is in the region between filaments. The maximum bending may be estimated in the following way. Let us say the compartment dimension of the cytoskeleton meshwork underlying the membrane is about 100 nm. As shown in figure S2a, taking the thickness of a single layer of antibodies to be 10 nm (Kienberger et al., 2004), the overall pre-assembled complex diameter would be maximally 100 nm. For the sake of argument, say each membrane (bilayer plus peripheral proteins) is ~ 10nm thick so the gold particle complex where a membrane partially wraps it has a radius of 60nm. The furthest the membrane–wrapped particle could "sink" between adjacent filaments (see figure S2a) would result in the membrane covering the gold-antibody complex with a "coverage area", CA, given by:

$$CA = 2\pi r^2(1-\cos\alpha), \qquad (1)$$

where α represents the half-angle corresponding to the contact area and r represents the radius of the whole complex (see figure S2a). For the

geometrical situation depicted in Figure S2a, $\alpha \leqq 56^\circ$. Assuming each binding site is saturated by the antibodies added in the next layer, the maximal number of surface Thy-1 bound to the particle then is calculated as:

Max. # bound Thy-1=600 X 2 X $2\pi r^2 (1-\cos\alpha)/4\pi r^2$ (2)

In (2), the number of available anti-Thy-1 antibodies on the particle was multiplied by 2 because of the bivalency of antibodies (total number bound=600). Given r = 60 nm, $1-\cos\alpha \leqq 0.45$, the maximum # of bound Thy-1 was calculated as $\leqq$ 135. Considering the possible inactivation by partial denaturation of anti-biotin antibodies during the coating process on the gold particles, the steric and orientation considerations preventing antibody binding, and whether the particle actually sinks to extent postulated in calculation, the actual number of Thy-1 bound to the pre-assembled complexes could be much less.

In equilibrium, the free energy gained from the antibody-antigen interaction should be greater than or equal to the energy required to bend the membrane to conform the membrane to the particle (E_{bend}). To bend an area of the membrane with an effective radius of curvature of 60 nm will require an energy given by:

$E_{bend}=Area*kc/(2*(r^2))$, (3)

where kc represents the bending modulus of cell membrane, r=radius of curvature, and the area is given by the calculation above in (1) (Sackmann, 1994). The local bending modulus will most likely lie somewhere between that for a bilayer where kc~28 k_BT at 37° C (Waugh et al., 1992) and that for the red cell membrane where kc~ $23k_BT$ (Evans, 1980). This leads to E_{bend}

values ranging from 40 k_BT if pure bilayer intervened between the cytoskeletal filaments (Sako and Kusumi, 1995) and 33 k_BT if the red cell membrane modulus is more appropriate. The energy released from antibody-antigen bond formation ranges from 11 kT to 22 k_BT at 37° C, corresponding to K_a values from 10^5 M^{-1} and 10^{10} M^{-1} (Van Regenmortel, 1998). Therefore, the free energy released from only 4 or fewer antibody-antigen bonds would be sufficient to bend the membrane to the extent required by the extreme model above.

While this paper was being reviewed, a publication concluded that so much energy is gained from ligand-receptor bonds that the plasma membrane would complete envelope a 100 nm diameter HIV particle (Sun and Wirtz, 2006). Our calculation assumes that complete envelopment of a coated 40nm gold particle would be frustrated by the presence of immediately subjacent cytoskeletal filaments. Then too, between transient anchorage points, gold particles diffuse rapidly which seems unlikely if they were completely enveloped.

Acknowledgement of the published work

This work was supported by NIH GM 41402 (KJ) and Cystic Fibrosis Foundation (SM). We thank G. Schuetz for helpful discussions.

Chapter 7: Future work

Several projects are ongoing to extend the work about transient anchorage, including verifying the working hypothesis described in Chapter 5 and mathematical modeling of transient anchorage based on stochastic chemical kinetics (figure 15).

To verify the working hypothesis, two approaches are taken: (1) the putative transient anchorage components are removed from the cellular system through RNAi silencing technology, drug inhibition or genetic knock-out methods. SPT results from these treatments will be used to evaluate the importance of specific components in transient anchorage. (2) Fluorescent SPT is being developed to acquire SPT movies in a fluorescent channel using quantum dots to replace gold particles, while the distribution of a specific fluorescently labeled putative transient anchorage component is imaged in a second channel. The coincidence of transient anchorage and enrichment of that specific transient anchorage component will provide evidence for its participation in the process.

Currently mouse fibroblasts permanently transfected with siRNA for CBP has been acquired from Dr. Christine Benistant. In addition, we have obtained preliminary data indicated phophatase inhibition may prolong the transient anchorage by several fold. Regarding the dynamic co-localization in fluorescent channels, images of CBP vs. SPT and caveolin-1 vs. SPT, as well as phosphor-SFK vs. SPT, have been obtained. The colocolization analysis is being performed.

We collaborate with Dr. Tim Elston, Dr. David Adalsteinsson, and Ms. Wanda Strychalski from Mathematics Department here at University of North Carolina, Chapel Hill to construct a plausible physical model based on ODEs in order to quantitatively describe transient anchorage and explain how the particuliar transient anchorage release time distribution is formed. A bi-exponential distribution is used as the fitting template for the real data. The model obtained depicts two states of transient anchorage. The model agrees with the real data in terms of the characteristic long-tail distribution of anchorage release times. Time series analysis will be employed to resolve the rate constants of the reactions involved in the formation of transient anchorage.

Figures and Tables

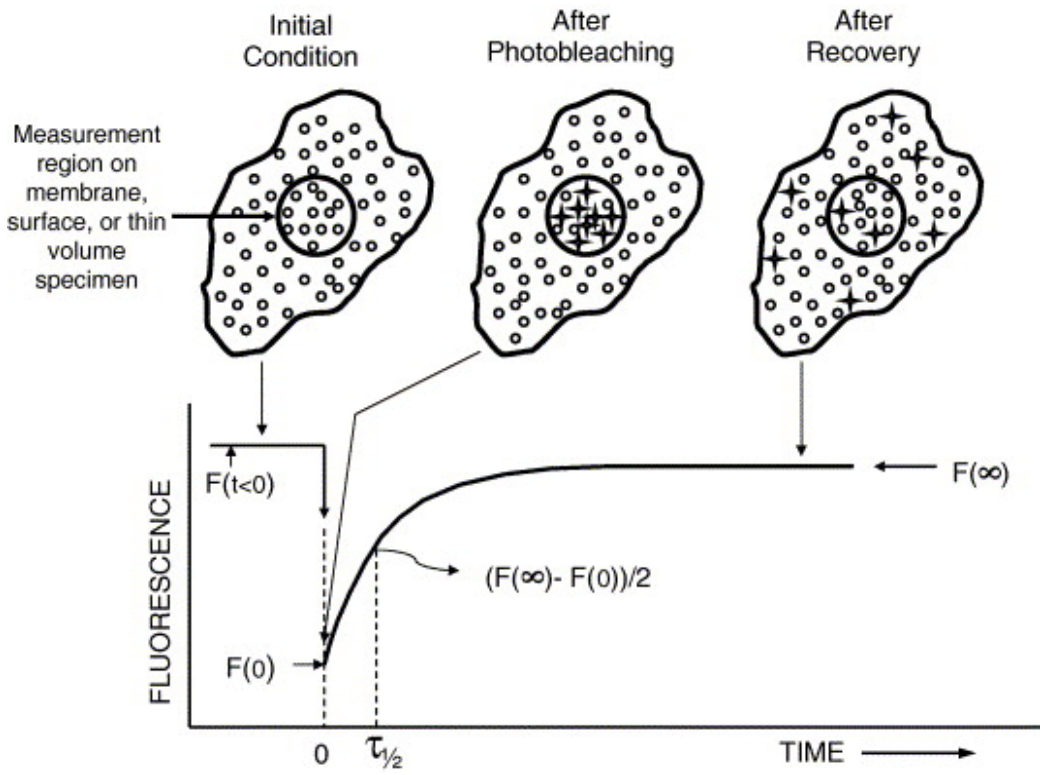

Fig. 1. Schematic of a FRAP experiment (see text for description of the FRAP experiment)

In the cartoon, o represents intact fluorophores, + represents bleached fluorophores.

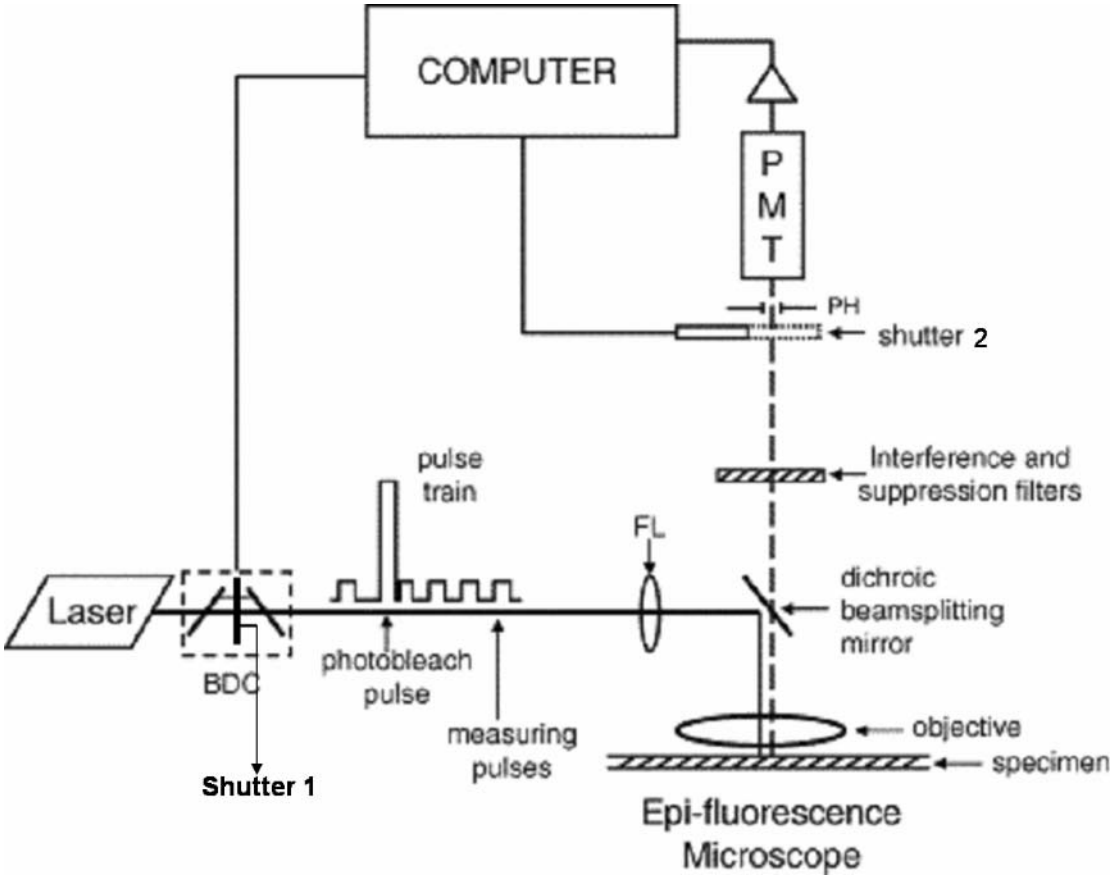

Fig. 2. Instrument schematic BDC: Beam divider and recombiner (see text).

FL: Convex lens to focus laser beam (see text). PMT: Photomultiplier card. PH: adjustable pinhole.

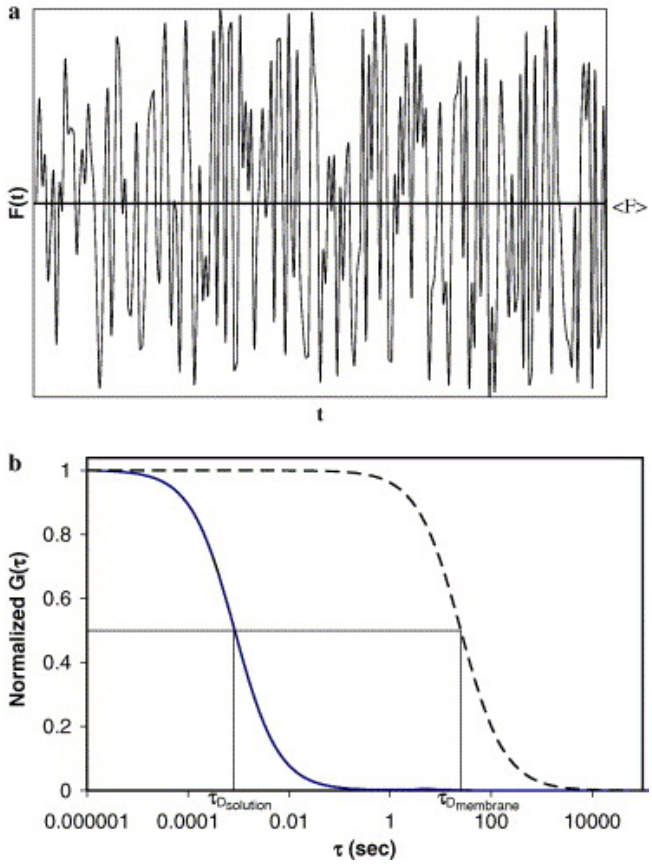

Fig. 3. Simulated fluorescence intensity raw data and calculated normalized aoutocorrelation function, G(τ).

(a) Example of fluorescence intensity fluctuations as a function of time also showing the time averaged fluorescence intensity, <F>.

(b) Normalized autocorrelation function, G(τ), was calculated for a free dye diffusing in solution ($D_{solution}$ = 300 μm^2/s; solid line) and a membrane marker diffusing laterally within a membrane ($D_{membrane}$ = 0.01 μm^2/s; dashed line) with r_o = 1 μm and z_o = 5 μm. For these values the diffusion times, $\tau_{Dsolution}$ and $\tau_{Dmembrane}$ are approximately 0.0008 and 25 s, respectively.

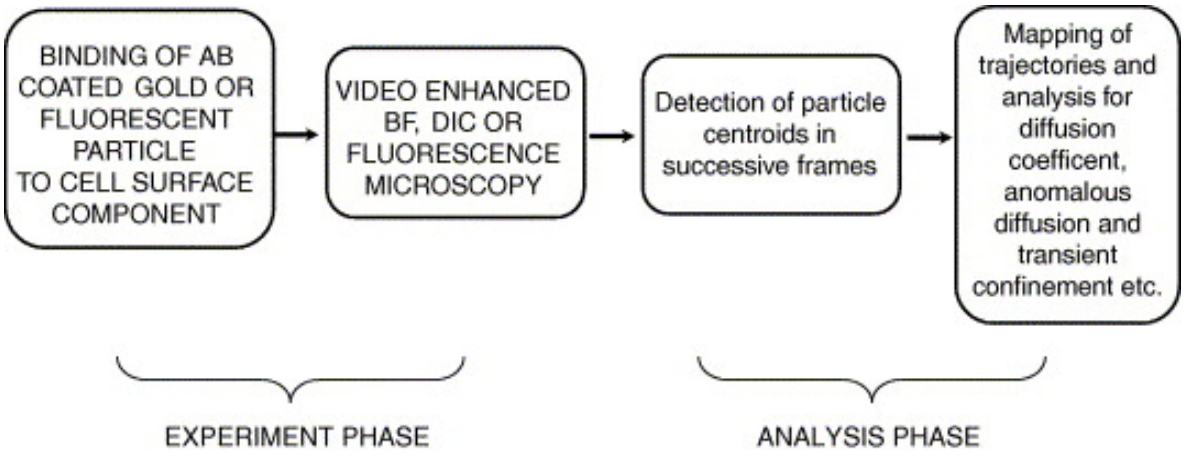

Fig. 4. Overall schematic of an SPT experiment.

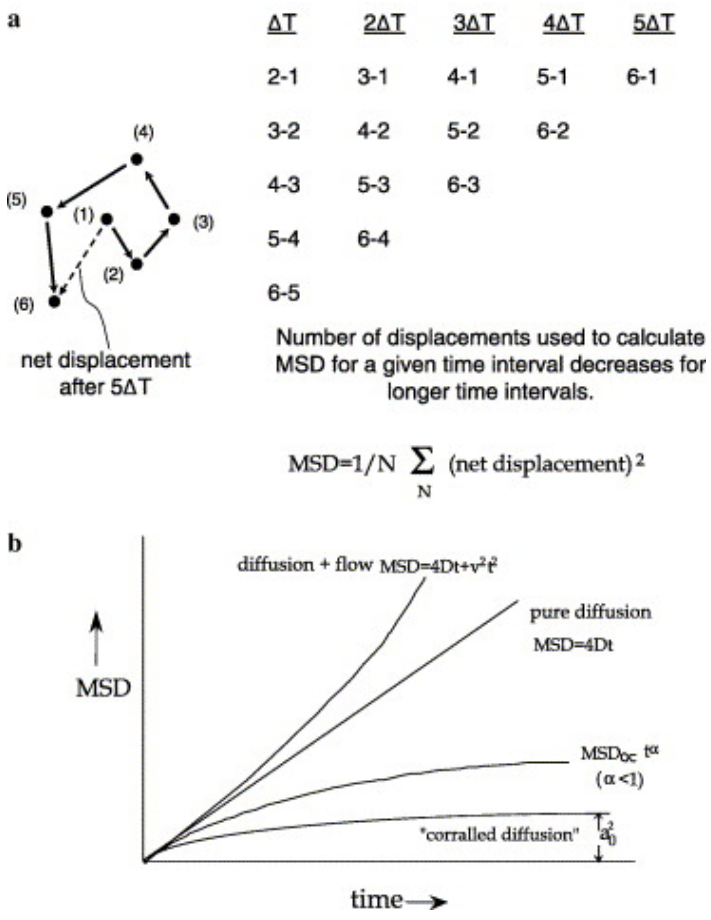

Fig. 5 Mean square displacement of lateral mobility.

(a) Schematic of how the mean square displacement (MSD) is calculated. ΔT represents the basic sampling interval (33 ms in the case of NTSC video standard).

(b) Schematic behavior of the MSD vs. time plots for pure diffusion in 2-dimensions, with a undirectioned flow of velocity, v, superimposed on random diffusion, anomalous sub-diffusion and corralled diffusion with in a circle of radius a_0.

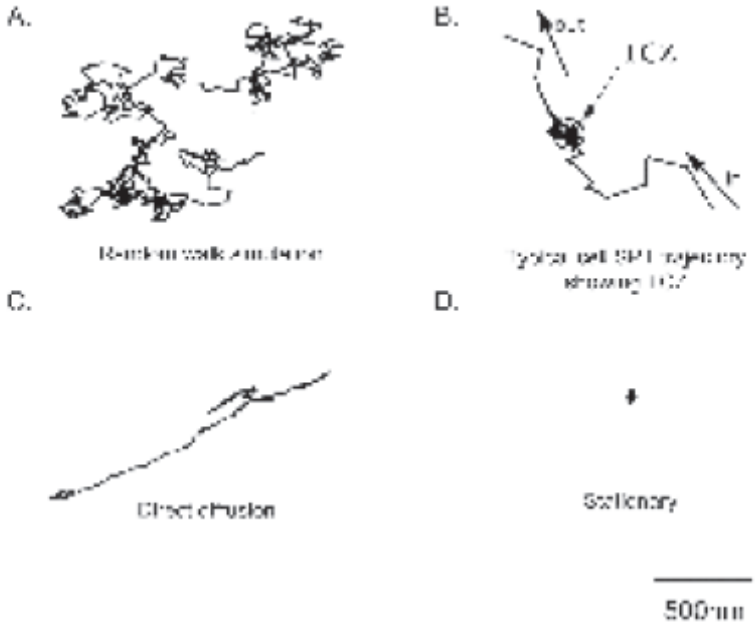

FIG. 6. Various trajectories from single-particle tracking (SPT) experiment on murine fibroblasts or simulation

(a) a typical 2-D random walk by computer simulation;

(b) a transient confinement zone (TCZ) is encountered when the particle diffuses on the cell membrane;

(c) directed movement;

(d) an anchored particle.

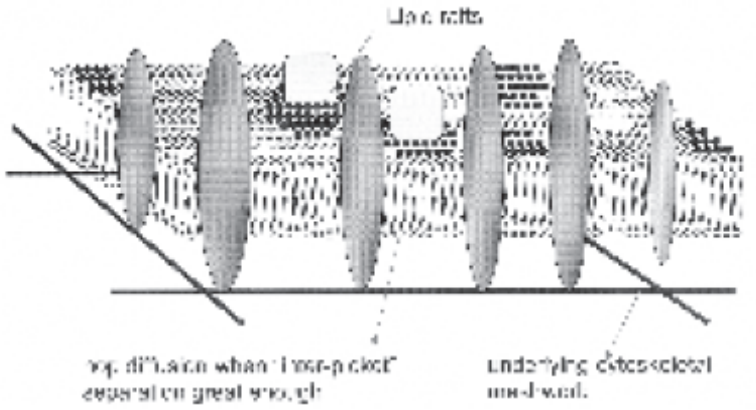

FIG. 7. Fence and picket structure of the plasma membrane model proposed by Ritchie et al. (28)

A schematic representation of the fundamental microstructure on cell membranes. The plasma membrane consists of a lipid bilayer with embedded proteins. These “picket” proteins are immobilized by being bound to the underlying actin-based cytoskeleton network and serve to separate the cell membrane into numerous small compartments. Mobile lipids and protein tissue within one compartment translocate to an adjacent one when fluctuations in the separation between pickets permit “hop diffusion.” Putative elementary lipid rafts (filled circles with tails) must disassemble on a time scale of milliseconds in order to allow raft proteins to “hop” to the adjacent compartment.

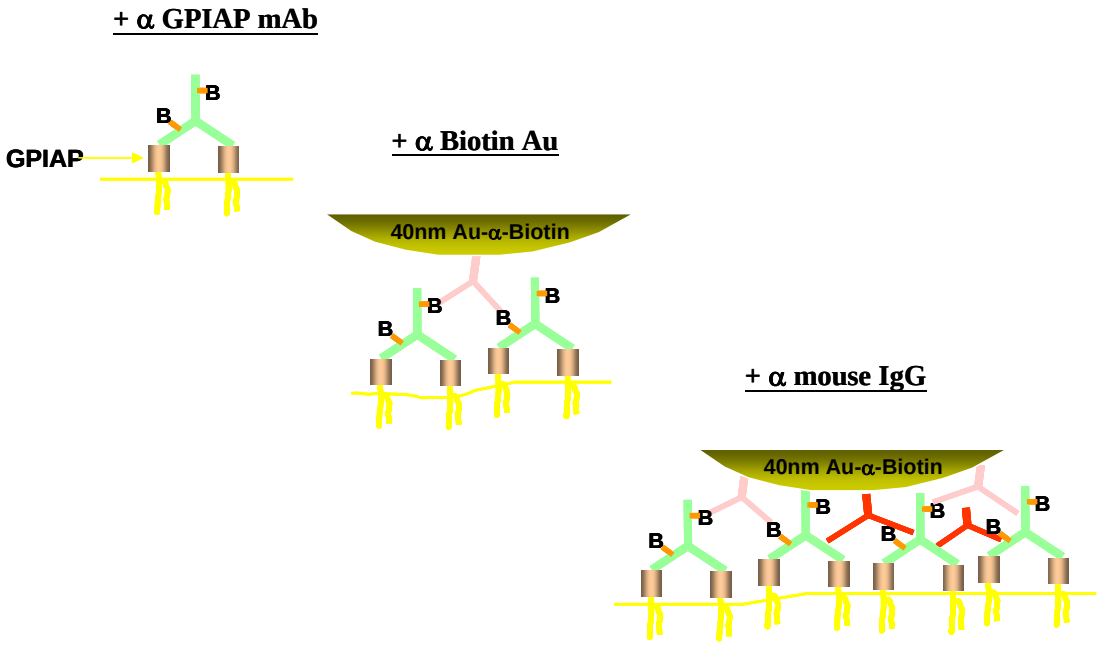

FIG. 8. Cross-linking scheme to cluster Thy-1 molecules on the cell surface:

Biotinylated anti-Thy1 mouse antibodies are first incubated with cells to bind to Thy1 molecules on the cell membrane. The gold particle is coated with anti-biotin antibodies, which can bind to biotinylated anti-Thy1 monoclonal antibodies, and then added on the cell membrane to form gold-antibody-antigen complex. The complex under the gold particle is further cross-linked by an anti-mouse IgG secondary antibody, presumably forming clusters of Thy1 molecules on the cell surface.

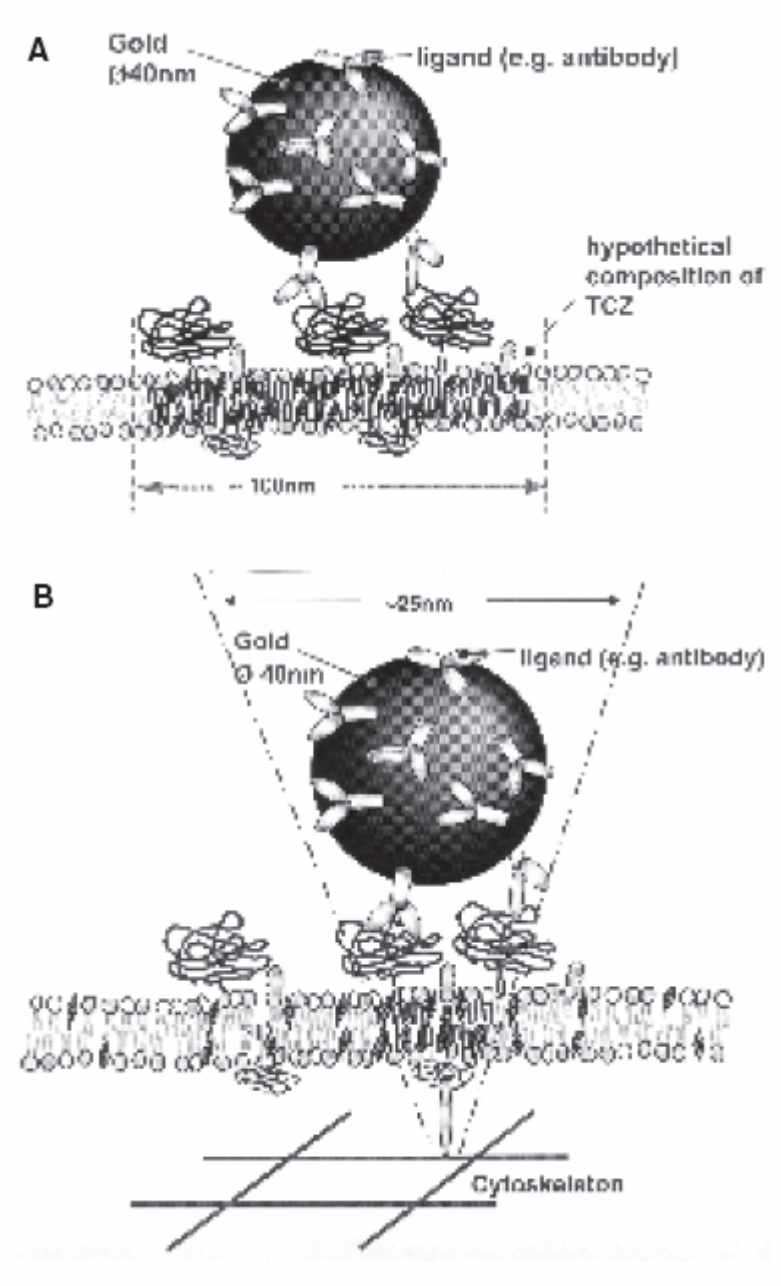

FIG. 9. Two different types of confinement induced by cross-linking.

(A) At lower levels of cross-linking, the gold particle diffuses within the transient confinement zone, which has a diameter of ~100 nm;

(B) at a higher level of cross-linking, the gold particle anchors to one spot for several seconds with a movement range of <25 nm due to temporary tethering to the cytoskeleton, mediated by Src family kinases.

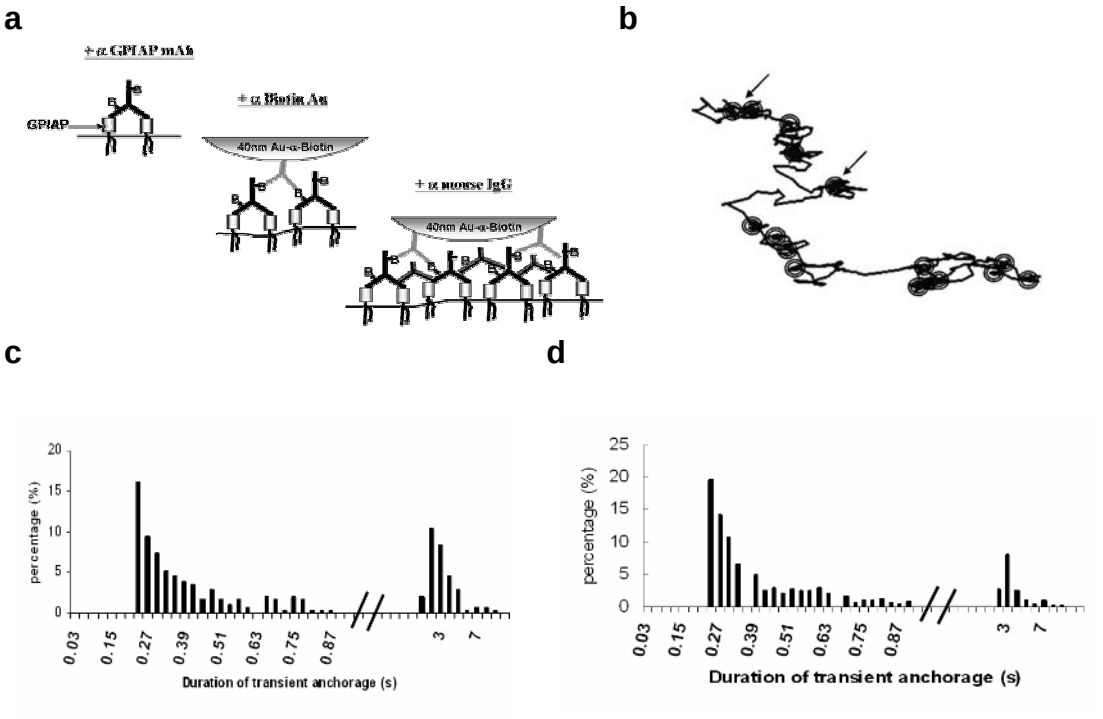

Figure 10: Maximal cross-linking scheme that produces transient anchorage.

(a) After incubating cells with biotinylated mouse primary antibodies recognizing specific GPI-anchored proteins (top), anti-biotin gold particles are added on the cell membrane to form bonds with the primary antibodies (middle). Finally, tertiary polyclonal antibodies that bind to mouse IgG are added to further cross-link the GPI-anchored proteins (bottom).

(b) During SPT, short periods with zero displacement were observed (arrows indicate representative transient anchorage events).

(c) The periods of transient anchorage for maximally cross-linked CD73 on IMR90 cells varied from several hundred milliseconds to more than ten seconds and are bimodally distributed.

(d) Pre-assembled complexes also showed a similar bimodal distribution of transient anchorage durations.

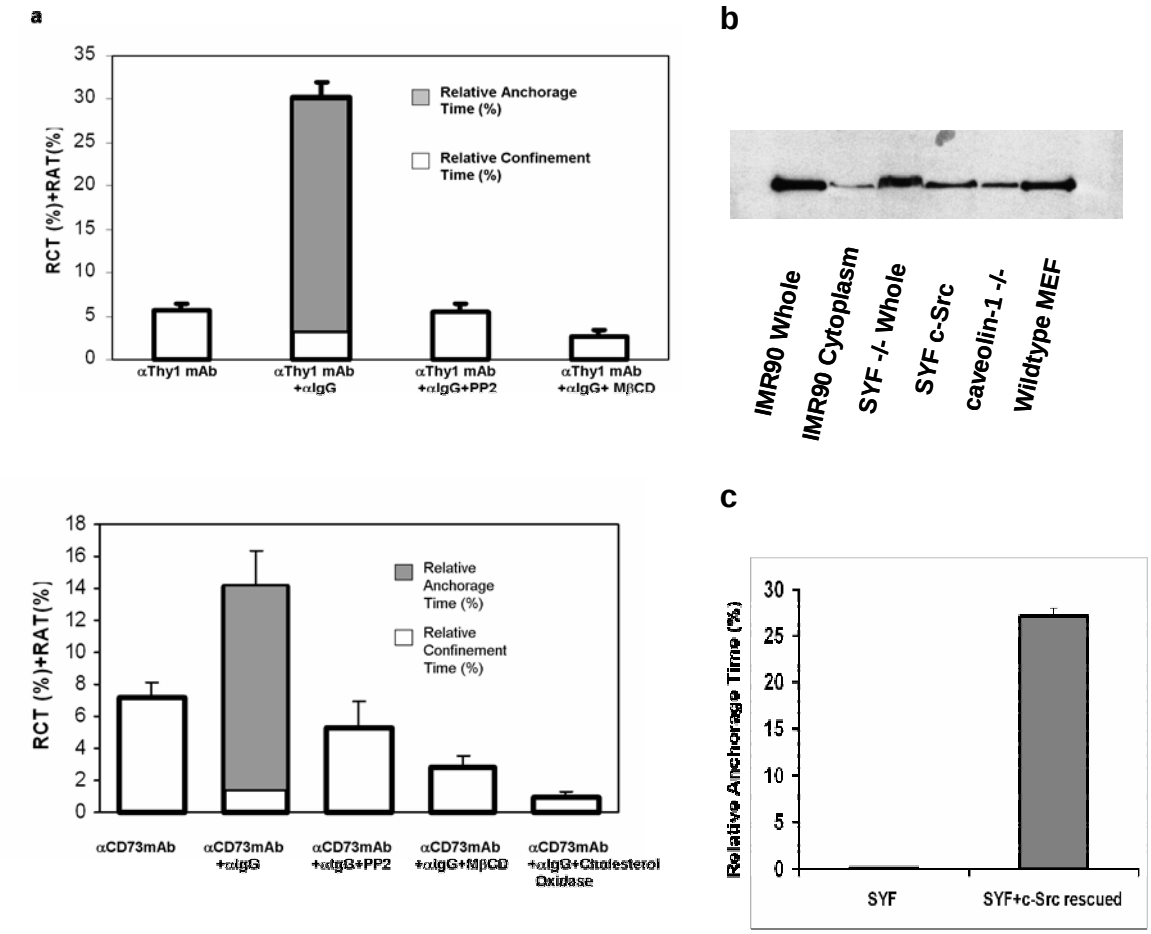

Figure 11: Both SFK inhibition and cholesterol depletion suppressed transient anchorage.

(a)C3H expressing Thy-1 (top) and IMR90 cells expressing CD73 (bottom) were treated with PP2 (n= 79 for Thy-1, n= 79 for CD73 where n is the number of trajectories analyzed; these were collected typically over 3 to 5 independent experiments) or cholesterol removing agents, mβCD (n= 100 for Thy-1, n= 70 for CD73)and/or cholesterol oxidase (n= 67 for CD 73), prior to maximal cross-linking. SPT with maximal cross-linking was the positive control (n= 90 for Thy-1, n= 88 for CD73). SPT without maximal cross-linking (without tertiary antibody addition) was the negative control (n= 69 for Thy-1, n= 85 for CD73). The error bars used here indicate the standard errors of the mean values (SEM).

(b) Western blotting was performed to check the expression of CD73 and whether the anti-human CD73 antibody can detect CD73 on the human and mouse cell lines used in the study.

(c) SFKs are required for transient anchorage of CD73. SFK deficient cells (n=65) did not demonstrate transient anchorage upon maximal cross-linking but transient anchorage can be rescued by transfection of c-Src (n=80) into the deficient cell line. The results were collected over 3 to 5 independent experiments.

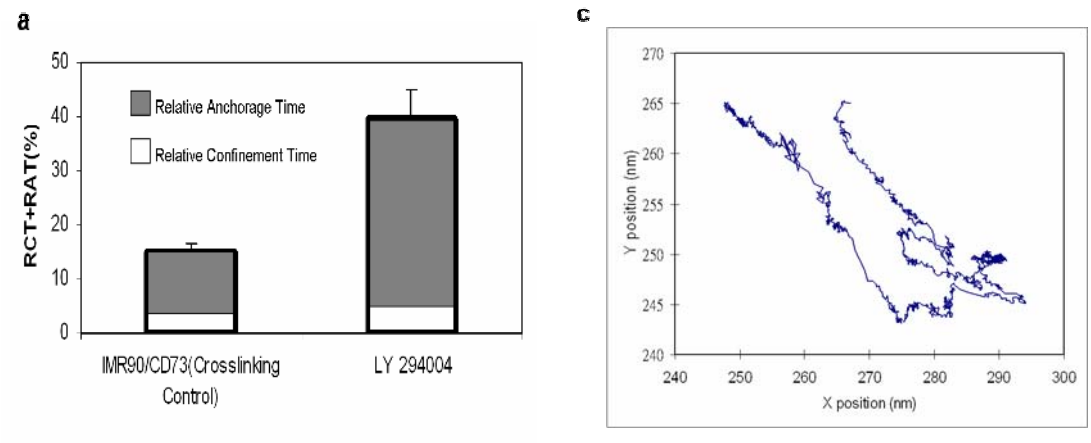

b

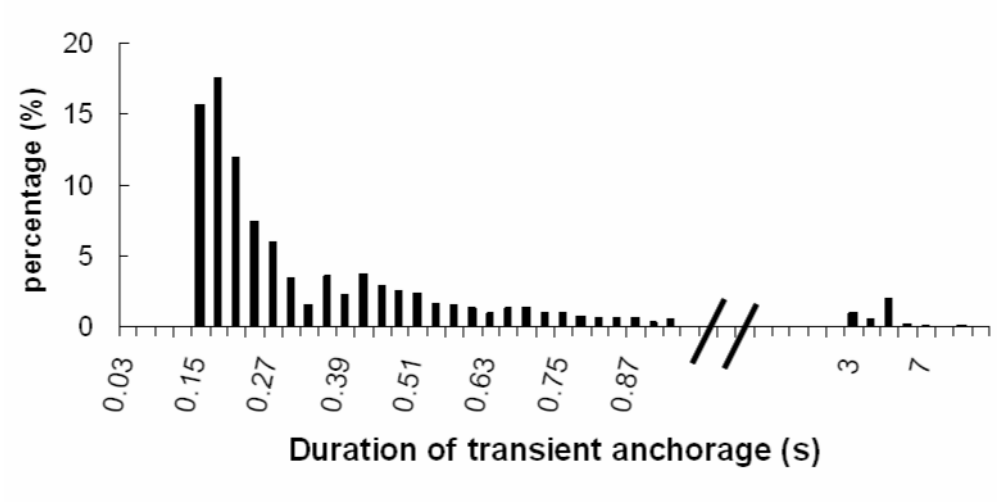

Figure 12: Effects of PI3 inhibition on transient anchorage.

(a) PI3 kinase inhibition induced more transient anchorage upon maximal cross-linking (n=117) compared with the control cells (n=120). The results were collected over 3 to 4 independent experiments. The error bars indicate the SEM.

(b)Compared to figure 11c, longer anchorage times were largely abolished in PI3 kinase inhibited cells.

(c) A portion of single particles after PI3 inhibition exhibited bi-directional movements as shown by this representative trajectory.

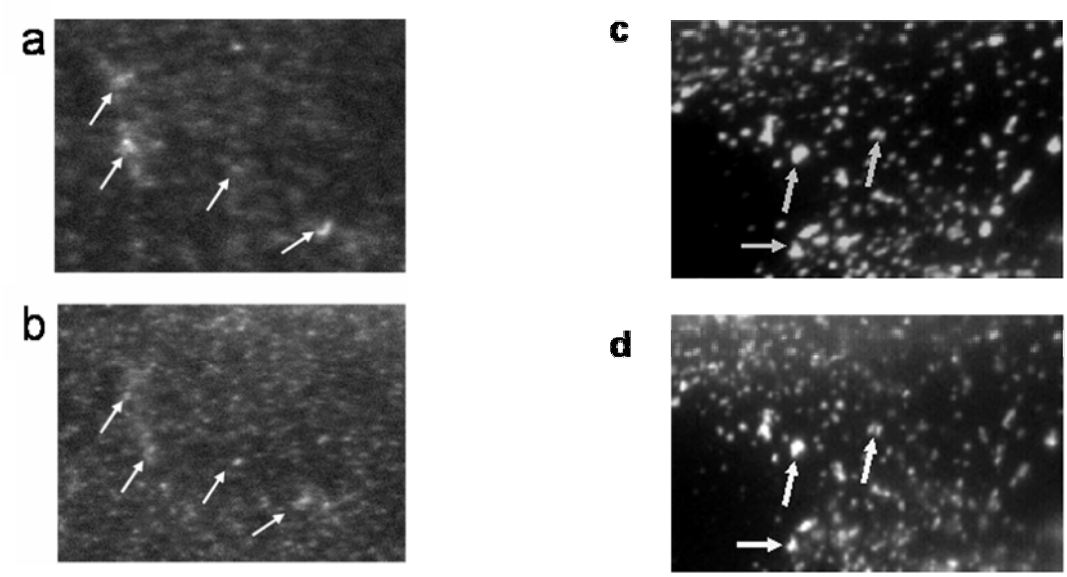

e

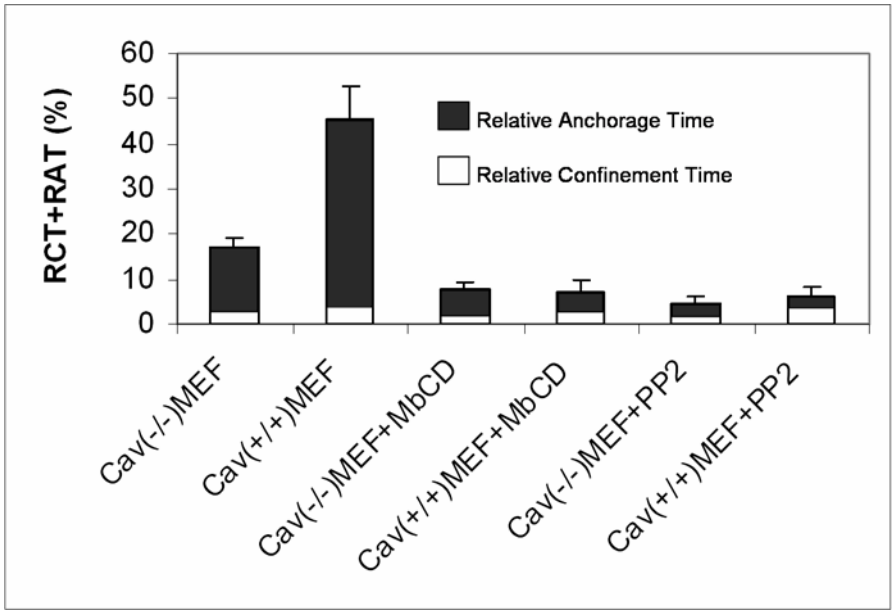

Figure 13: Caveolae participated in transient anchorage.

(a-b) Partial co-localization between CD73 (a) and caveolin-1 (b) was seen on IMR 90 cells after maximal cross-linking. Arrows show representative regions of colocalization.

(c-d) Partial co-localization between Thy-1 (c) and caveolin-1 (d) was seen on C3H cells after maximal-cross-linking. Arrows show representative regions of colocalization. The specificity of antibodies used here has been examined by the manufacturers and antibodies described above do not cross-react.

(e) In Caveolin-1 deficient mouse embryonic cells (n=92), transient anchorage of Thy-1was reduced to about one third compared to wildtype parental cells (n=100). Transient anchorage could be suppressed by SFK inhibition and cholesterol depletion in both cell lines (n= 70 for cav-/- +MBCD, n=72 for

cav+/+ +MBCD, n= 88 for cav-/- +pp2, n= 75 for cav+/+ +pp2) The results were collected over 3 to 5 independent experiemnts. The error bars indicate the SEM.

a

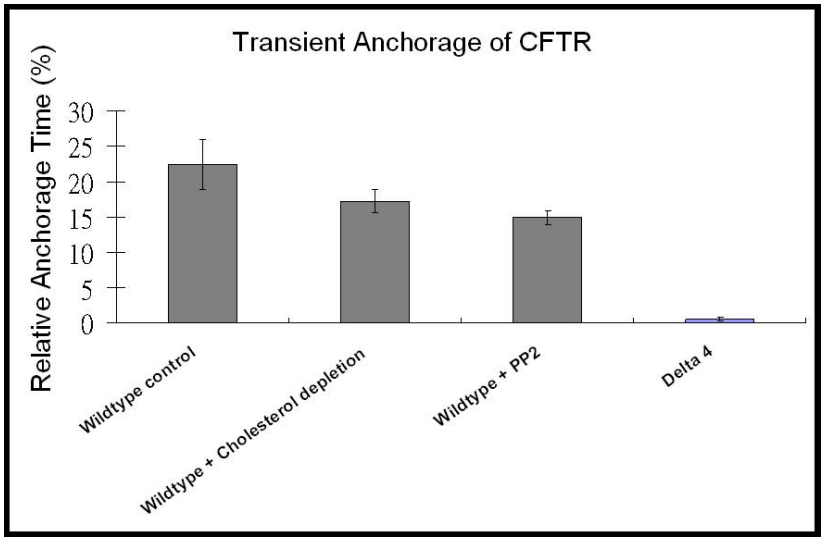

b

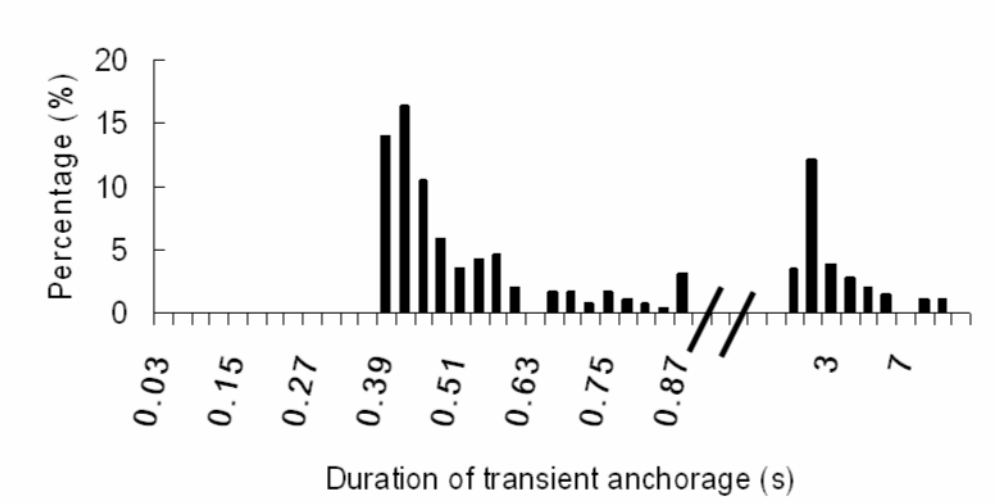

Figure 14: CFTR demonstrated transient anchorage independent of maximal cross-linking, SFK activities and cholesterol presence.

(a) CFTR tagged with an extracellular HA-epitope was expressed in C3H cells and labeled with biotinylated anti-HA antibodies and anti-biotin antibody conjugated gold for SPT. CFTR displayed transient anchorage in the absence of tertiary cross-linking antibody. SFK inhibition (by PP2) or cholesterol depletion (by MβCD) only slightly reduced the transient anchorage, while deletion of the PDZ binding domain in CFTR (delta 4 mutant) caused transient anchorage to be almost completely eliminated. The error bars indicate the SEM.

(b) CFTR demonstrated a similar bimodal distribution of transient anchorage

durations compared to the maximal-linked CD73 in figure 12(c).

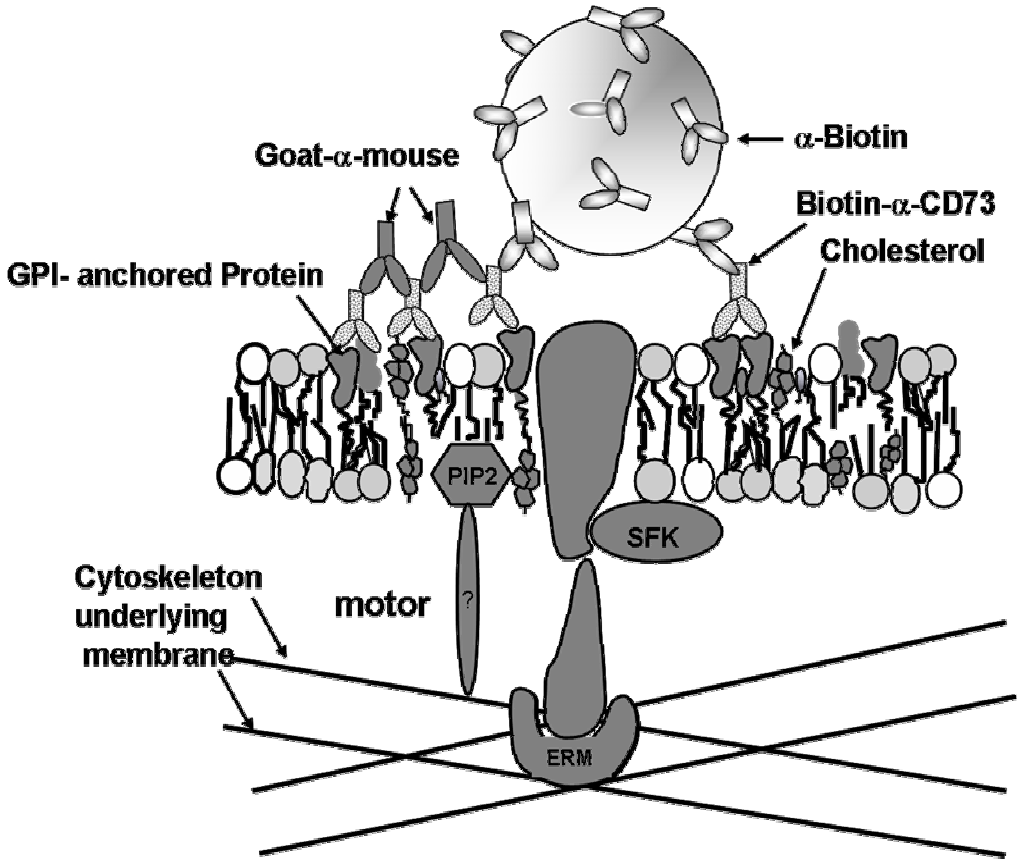

Figure 15: Transient anchorage hypothesis.

Cross-linking causes nanodomains to form on both inner and outer-leaflet, with a transmembrane protein bridging the two leaflets to transduce the signal. When an activated SFK randomly partitions into such a nanodomain, the phosphorylation by the SFK causes a resident molecule, possibly the transmembrane protein, to attach to the actin cytoskeleton indirectly through other linker proteins. The attachment results in a transient anchorage until the SFK becomes deactivated and a recruited phosphatase dephosphorylates the linking resident molecule in the nanodomain (see discussion for details). ERM: moesin/ezrin/radixin proteins. PIP2: phosphatidyl inositol bisphosphate. SFK: Src family kinase.

Table 1

Dependence of CD73 transient anchorage on dilution of the tertiary antibody

Dilution ratio [a]	1:2000	1:1000	1:200	1:100	1:50
Total confinement (%), [b]	7.0±1.0	10.8±1.7	15.1±2.7	36.8±2.4	14.5±2.0
RCT (%)	7.0±1.0	10.8±1.7	7.2±0.1	15.0±1.7	10.7±1.7
RAT(%)	Not Detected	Not Detected	12.2±1.6	31.4±2.2	11.5±1.1

[a] Concentration of stock solution = 2 mg/ml

[b] To avoid overestimation, the total confinement is obtained by adding RCT and RAT then subtracting the overlapping time in which transient anchorage and TCZs both occurred

Reference

Axelrod, D., D.E. Koppel, J. Schlessinger, E. Elson, and W.W. Webb. 1976. Mobility measurement by analysis of fluorescence photobleaching recovery kinetics. *Biophys J*. 16:1055-69.

Bacia, K., D. Scherfeld, N. Kahya, and P. Schwille. 2004. Fluorescence correlation spectroscopy relates rafts in model and native membranes. *Biophys J*. 87:1034-43.

Bacia, K., and P. Schwille. 2003. A dynamic view of cellular processes by in vivo fluorescence auto- and cross-correlation spectroscopy. *Methods*. 29:74-85.

Berland, K.M., P.T. So, and E. Gratton. 1995. Two-photon fluorescence correlation spectroscopy: method and application to the intracellular environment. *Biophys J*. 68:694-701.

Bose, G., P. Schwille, and T. Lamparter. 2004. The mobility of phytochrome within protonemal tip cells of the moss Ceratodon purpureus, monitored by fluorescence correlation spectroscopy. *Biophys J*. 87:2013-21.

Brown, D.A., and E. London. 1997. Structure of detergent-resistant membrane domains: does phase separation occur in biological membranes? *Biochem Biophys Res Commun*. 240:1-7.

Brown, D.A., and E. London. 1998. Functions of lipid rafts in biological membranes. *Annu Rev Cell Dev Biol*. 14:111-36.

Brown, D.A., and J.K. Rose. 1992. Sorting of GPI-anchored proteins to glycolipid-enriched membrane subdomains during transport to the apical cell surface. *Cell*. 68:533-44.

Chen, Y., B. Yang, and K. Jacobson. 2004. Transient confinement zones: a type of lipid raft? *Lipids*. 39:1115-9.

Coyne, C.B., and J.M. Bergelson. 2006. Virus-induced Abl and Fyn kinase signals permit coxsackievirus entry through epithelial tight junctions. *Cell*. 124:119-31.

Damm, E.M., L. Pelkmans, J. Kartenbeck, A. Mezzacasa, T. Kurzchalia, and A. Helenius. 2005. Clathrin- and caveolin-1-independent endocytosis: entry of simian virus 40 into cells devoid of caveolae. *J Cell Biol*. 168:477-88.

Daumas, F., N. Destainville, C. Millot, A. Lopez, D. Dean, and L. Salome. 2003a. Confined diffusion without fences of a g-protein-coupled receptor as revealed by single particle tracking. *Biophys J*. 84:356-66.

Daumas, F., N. Destainville, C. Millot, A. Lopez, D. Dean, and L. Salome. 2003b. Interprotein interactions are responsible for the confined diffusion of a G-protein-coupled receptor at the cell surface. *Biochem Soc Trans*. 31:1001-5.

Dietrich, C., Z.N. Volovyk, M. Levi, N.L. Thompson, and K. Jacobson. 2001. Partitioning of Thy-1, GM1, and cross-linked phospholipid analogs into lipid rafts reconstituted in supported model membrane monolayers. *Proc Natl Acad Sci U S A*. 98:10642-7.

Dietrich, C., B. Yang, T. Fujiwara, A. Kusumi, and K. Jacobson. 2002. Relationship of lipid rafts to transient confinement zones detected by single particle tracking. *Biophys J*. 82:274-84.

Dreja, K., M. Voldstedlund, J. Vinten, J. Tranum-Jensen, P. Hellstrand, and K. Sward. 2002. Cholesterol depletion disrupts caveolae and differentially impairs agonist-induced arterial contraction. *Arterioscler Thromb Vasc Biol*. 22:1267-72.

Durrheim, G.A., D. Garnett, K.M. Dennehy, and A.D. Beyers. 2001. Thy-1 associated pp85--90 is a potential docking site for SH2 domain-containing signal transduction molecules. *Cell Biol Int*. 25:33-42.

Elson, E.L. 2004. Quick tour of fluorescence correlation spectroscopy from its inception. *J Biomed Opt*. 9:857-64.

Elson, E.L., and H. Qian. 1989. Interpretation of fluorescence correlation spectroscopy and photobleaching recovery in terms of molecular interactions. *Methods Cell Biol*. 30:307-32.

Evans, E.A. 1980. Minimum energy analysis of membrane deformation applied to pipet aspiration and surface adhesion of red blood cells. *Biophys J*. 30:265-84.

Ewers, H., A.E. Smith, I.F. Sbalzarini, H. Lilie, P. Koumoutsakos, and A. Helenius. 2005. Single-particle tracking of murine polyoma virus-like particles on live cells and artificial membranes. *Proc Natl Acad Sci U S A*. 102:15110-5.

Felsenfeld, D.P., D. Choquet, and M.P. Sheetz. 1996. Ligand binding regulates the directed movement of beta1 integrins on fibroblasts. *Nature*. 383:438-40.

Fievet, B.T., A. Gautreau, C. Roy, L. Del Maestro, P. Mangeat, D. Louvard, and M. Arpin. 2004. Phosphoinositide binding and phosphorylation act sequentially in the activation mechanism of ezrin. *J Cell Biol*. 164:653-9.

Fujiwara, T., K. Ritchie, H. Murakoshi, K. Jacobson, and A. Kusumi. 2002. Phospholipids undergo hop diffusion in compartmentalized cell membrane. *J Cell Biol*. 157:1071-81.

Gelles, J., B.J. Schnapp, and M.P. Sheetz. 1988. Tracking kinesin-driven movements with nanometre-scale precision. *Nature*. 331:450-3.

Gentzsch, M., X.B. Chang, L. Cui, Y. Wu, V.V. Ozols, A. Choudhury, R.E. Pagano, and J.R. Riordan. 2004. Endocytic trafficking routes of wild type and DeltaF508 cystic fibrosis transmembrane conductance regulator. *Mol Biol Cell*. 15:2684-96.

Gordon, G.W., B. Chazotte, X.F. Wang, and B. Herman. 1995. Analysis of simulated and experimental fluorescence recovery after photobleaching. Data for two diffusing components. *Biophys J*. 68:766-78.

Harder, T., and K. Simons. 1999. Clusters of glycolipid and glycosylphosphatidylinositol-anchored proteins in lymphoid cells: accumulation of actin regulated by local tyrosine phosphorylation. *Eur J Immunol*. 29:556-62.

Haustein, E., and P. Schwille. 2004. Single-molecule spectroscopic methods. *Curr Opin Struct Biol*. 14:531-40.

Heerklotz, H. 2002. Triton promotes domain formation in lipid raft mixtures. *Biophys J*. 83:2693-701.

Hegener, O., L. Prenner, F. Runkel, S.L. Baader, J. Kappler, and H. Haberlein. 2004. Dynamics of beta2-adrenergic receptor-ligand complexes on living cells. *Biochemistry*. 43:6190-9.

Hess, S.T., and W.W. Webb. 2002. Focal volume optics and experimental artifacts in confocal fluorescence correlation spectroscopy. *Biophys J*. 83:2300-17.

Holifield, B.F., A. Ishihara, and K. Jacobson. 1990. Comparative behavior of membrane protein-antibody complexes on motile fibroblasts: implications for a mechanism of capping. *J Cell Biol*. 111:2499-512.

Itoh, K., M. Sakakibara, S. Yamasaki, A. Takeuchi, H. Arase, M. Miyazaki, N. Nakajima, M. Okada, and T. Saito. 2002. Cutting edge: negative regulation of immune synapse formation by anchoring lipid raft to cytoskeleton through Cbp-EBP50-ERM assembly. *J Immunol*. 168:541-4.

Jacobson, K., and C. Dietrich. 1999. Looking at lipid rafts? *Trends Cell Biol*. 9:87-91.

Jacobson, K., A. Ishihara, and R. Inman. 1987. Lateral diffusion of proteins in membranes. *Annu Rev Physiol*. 49:163-75.

Jacobson, K., E.D. Sheets, and R. Simson. 1995. Revisiting the fluid mosaic model of membranes. *Science*. 268:1441-2.

Janes, P.W., S.C. Ley, and A.I. Magee. 1999. Aggregation of lipid rafts accompanies signaling via the T cell antigen receptor. *J Cell Biol*. 147:447-61.

Kahya, N., D. Scherfeld, K. Bacia, B. Poolman, and P. Schwille. 2003. Probing lipid mobility of raft-exhibiting model membranes by fluorescence correlation spectroscopy. *J Biol Chem*. 278:28109-15.

Kahya, N., D. Scherfeld, K. Bacia, and P. Schwille. 2004. Lipid domain formation and dynamics in giant unilamellar vesicles explored by fluorescence correlation spectroscopy. *J Struct Biol*. 147:77-89.

Kapitza, H.G., G. McGregor, and K.A. Jacobson. 1985. Direct measurement of lateral transport in membranes by using time-resolved spatial photometry. *Proc Natl Acad Sci U S A*. 82:4122-6.

Kenworthy, A.K., N. Petranova, and M. Edidin. 2000. High-resolution FRET microscopy of cholera toxin B-subunit and GPI-anchored proteins in cell plasma membranes. *Mol Biol Cell*. 11:1645-55.

Kienberger, F., H. Mueller, V. Pastushenko, and P. Hinterdorfer. 2004. Following single antibody binding to purple membranes in real time. *EMBO Rep*. 5:579-83.

Koppel, D.E. 1979. Fluorescence redistribution after photobleaching. A new multipoint analysis of membrane translational dynamics. *Biophys J*. 28:281-91.

Koppel, D.E., D. Axelrod, J. Schlessinger, E.L. Elson, and W.W. Webb. 1976. Dynamics of fluorescence marker concentration as a probe of mobility. *Biophys J*. 16:1315-29.

Korlach, J., P. Schwille, W.W. Webb, and G.W. Feigenson. 1999. Characterization of lipid bilayer phases by confocal microscopy and fluorescence correlation spectroscopy. *Proc Natl Acad Sci U S A*. 96:8461-6.

Krauss, K., and P. Altevogt. 1999. Integrin leukocyte function-associated antigen-1-mediated cell binding can be activated by clustering of membrane rafts. *J Biol Chem*. 274:36921-7.

Kroczek, R.A., K.C. Gunter, B. Seligmann, and E.M. Shevach. 1986. Induction of T cell activation by monoclonal anti-Thy-1 antibodies. *J Immunol*. 136:4379-84.

Kural, C., H. Kim, S. Syed, G. Goshima, V.I. Gelfand, and P.R. Selvin. 2005. Kinesin and dynein move a peroxisome in vivo: a tug-of-war or coordinated movement? *Science*. 308:1469-72.

Kusumi, A. 2004. Single Molecule Imaging of Raft Dynamics and Raft-based Signal Transductionin Living Cells. *Biophysical Society Meeting (Special Discussion)*.

Kusumi, A., H. Ike, C. Nakada, K. Murase, and T. Fujiwara. 2005. Single-molecule tracking of membrane molecules: plasma membrane compartmentalization and dynamic assembly of raft-philic signaling molecules. *Semin Immunol*. 17:3-21.

Kusumi, A., I. Koyama-Honda, and K. Suzuki. 2004. Molecular dynamics and interactions for creation of stimulation-induced stabilized rafts from small unstable steady-state rafts. *Traffic*. 5:213-30.

Lee, G.M., A. Ishihara, and K.A. Jacobson. 1991. Direct observation of brownian motion of lipids in a membrane. *Proc Natl Acad Sci U S A*. 88:6274-8.

Lee, G.M., F. Zhang, A. Ishihara, C.L. McNeil, and K.A. Jacobson. 1993. Unconfined lateral diffusion and an estimate of pericellular matrix viscosity revealed by measuring the mobility of gold-tagged lipids. *J Cell Biol*. 120:25-35.

Lee, S.H., J. Jacobson, D. Trudell, and D. Resnick. 1998. Ligaments of the ankle: normal anatomy with MR arthrography. *J Comput Assist Tomogr*. 22:807-13.

Levin, M.K., and J.H. Carson. 2004. Fluorescence correlation spectroscopy and quantitative cell biology. *Differentiation*. 72:1-10.

Lidke, D.S., K.A. Lidke, B. Rieger, T.M. Jovin, and D.J. Arndt-Jovin. 2005. Reaching out for signals: filopodia sense EGF and respond by directed retrograde transport of activated receptors. *J Cell Biol*. 170:619-26.

Lieto, A.M., R.C. Cush, and N.L. Thompson. 2003. Ligand-receptor kinetics measured by total internal reflection with fluorescence correlation spectroscopy. *Biophys J*. 85:3294-302.

Lippincott-Schwartz, J., E. Snapp, and A. Kenworthy. 2001. Studying protein dynamics in living cells. *Nat Rev Mol Cell Biol*. 2:444-56.

Magde, D. *Physical Review Letters*. 29:705.

Magde, D., E.L. Elson, and W.W. Webb. 1974. Fluorescence correlation spectroscopy. II. An experimental realization. *Biopolymers*. 13:29-61.

Malinska, K., J. Malinsky, M. Opekarova, and W. Tanner. 2003. Visualization of protein compartmentation within the plasma membrane of living yeast cells. *Mol Biol Cell*. 14:4427-36.

Marsh, M., and A. Helenius. 2006. Virus entry: open sesame. *Cell*. 124:729-40.

Matsuoka, H., S. Nada, and M. Okada. 2004. Mechanism of Csk-mediated down-regulation of Src family tyrosine kinases in epidermal growth factor signaling. *J Biol Chem*. 279:5975-83.

Mayor, S., K.G. Rothberg, and F.R. Maxfield. 1994. Sequestration of GPI-anchored proteins in caveolae triggered by cross-linking. *Science*. 264:1948-51.

Meier, J., C. Vannier, A. Serge, A. Triller, and D. Choquet. 2001. Fast and reversible trapping of surface glycine receptors by gephyrin. *Nat Neurosci*. 4:253-60.

Murase, K., T. Fujiwara, Y. Umemura, K. Suzuki, R. Iino, H. Yamashita, M. Saito, H. Murakoshi, K. Ritchie, and A. Kusumi. 2004a. Ultrafine membrane compartments for molecular diffusion as revealed by single molecule techniques. *Biophys J*. 86:4075-93.

Murase, K., T. Fujiwara, Y. Umemura, K. Suzuki, R. Iino, H. Yamashita, M. Saito, H. Murakoshi, K. Ritchie, and A. Kusumi. 2004b. Ultrafine Membrane Compartments for Molecular Diffusion as Revealed by Single Molecule Techniques. *Biophys J*. 86:4075-4093.

Parpal, S., M. Karlsson, H. Thorn, and P. Stralfors. 2001. Cholesterol depletion disrupts caveolae and insulin receptor signaling for metabolic control via insulin receptor substrate-1, but not for mitogen-activated protein kinase control. *J Biol Chem*. 276:9670-8.

Pelkmans, L., D. Puntener, and A. Helenius. 2002. Local actin polymerization and dynamin recruitment in SV40-induced internalization of caveolae. *Science*. 296:535-9.

Petersen, N.O., and E.L. Elson. 1986. Measurements of diffusion and chemical kinetics by fluorescence photobleaching recovery and fluorescence correlation spectroscopy. *Methods Enzymol*. 130:454-84.

Petersen, N.O., S. Felder, and E.L. Elson. 1986. Measurement of lateral diffusion by fluorescence photobleaching recovery. *In* Handbook of Experimental Immunology. D.M. Weir, editor. Blackwell Scientific Publishers, New York.

Politz, J.C., E.S. Browne, D.E. Wolf, and T. Pederson. 1998. Intranuclear diffusion and hybridization state of oligonucleotides measured by fluorescence correlation spectroscopy in living cells. *Proc Natl Acad Sci U S A*. 95:6043-8.

Qian, H., M.P. Sheetz, and E.L. Elson. 1991. Single particle tracking. Analysis of diffusion and flow in two-dimensional systems. *Biophys J*. 60:910-21.

Raff, M.C., M. Sternberg, and R.B. Taylor. 1970. Immunoglobulin determinants on the surface of mouse lymphoid cells. *Nature*. 225:553-4.

Raghuram, V., H. Hormuth, and J.K. Foskett. 2003. A kinase-regulated mechanism controls CFTR channel gating by disrupting bivalent PDZ domain interactions. *Proc Natl Acad Sci U S A*. 100:9620-5.

Rao, M., and S. Mayor. 2005. Use of Forster's resonance energy transfer microscopy to study lipid rafts. *Biochim Biophys Acta*. 1746:221-33.

Rigler, R., and E. Elson. 2001. Fluorescence Correlation Spectroscopy: Theory and Applications. Springer, Berlin.

Ritchie, K., R. Iino, T. Fujiwara, K. Murase, and A. Kusumi. 2003. The fence and picket structure of the plasma membrane of live cells as revealed by single molecule techniques (Review). *Mol Membr Biol*. 20:13-8.

Sackmann, E. 1994. Membrane bending energy concept of vesicle- and cell-shapes and shape-transitions. *FEBS Letters*. 346:3-16.

Sako, Y., and A. Kusumi. 1995. Barriers for lateral diffusion of transferrin receptor in the plasma membrane as characterized by receptor dragging by laser tweezers: fence versus tether. *J Cell Biol*. 129:1559-74.

Saxton, M.J. 1993. Lateral diffusion in an archipelago. Single-particle diffusion. *Biophys J*. 64:1766-80.

Saxton, M.J., and K. Jacobson. 1997. Single-particle tracking: applications to membrane dynamics. *Annu Rev Biophys Biomol Struct*. 26:373-99.

Schuck, S., M. Honsho, K. Ekroos, A. Shevchenko, and K. Simons. 2003. Resistance of cell membranes to different detergents. *Proc Natl Acad Sci U S A*. 100:5795-800.

Schwille, P., U. Haupts, S. Maiti, and W.W. Webb. 1999a. Molecular dynamics in living cells observed by fluorescence correlation spectroscopy with one- and two-photon excitation. *Biophys J*. 77:2251-65.

Schwille, P., J. Korlach, and W.W. Webb. 1999b. Fluorescence correlation spectroscopy with single-molecule sensitivity on cell and model membranes. *Cytometry*. 36:176-82.

Sharma, P., R. Varma, R.C. Sarasij, Ira, K. Gousset, G. Krishnamoorthy, M. Rao, and S. Mayor. 2004. Nanoscale organization of multiple GPI-anchored proteins in living cell membranes. *Cell*. 116:577-89.

Sheets, E.D., G.M. Lee, R. Simson, and K. Jacobson. 1997. Transient confinement of a glycosylphosphatidylinositol-anchored protein in the plasma membrane. *Biochemistry*. 36:12449-58.

Sheetz, M.P., S. Turney, H. Qian, and E.L. Elson. 1989. Nanometre-level analysis demonstrates that lipid flow does not drive membrane glycoprotein movements. *Nature*. 340:284-8.

Shogomori, H., and D.A. Brown. 2003. Use of detergents to study membrane rafts: the good, the bad, and the ugly. *Biol Chem*. 384:1259-63.

Short, D.B., K.W. Trotter, D. Reczek, S.M. Kreda, A. Bretscher, R.C. Boucher, M.J. Stutts, and S.L. Milgram. 1998. An apical PDZ protein anchors the cystic fibrosis transmembrane conductance regulator to the cytoskeleton. *J Biol Chem*. 273:19797-801.

Simons, K., and E. Ikonen. 1997. Functional rafts in cell membranes. *Nature*. 387:569-72.

Simons, K., and E. Ikonen. 2000. How cells handle cholesterol. *Science*. 290:1721-6.

Simons, K., and D. Toomre. 2000. Lipid rafts and signal transduction. *Nat Rev Mol Cell Biol*. 1:31-9.

Simons, K., and G. van Meer. 1988. Lipid sorting in epithelial cells. *Biochemistry*. 27:6197-202.

Simson, R., E.D. Sheets, and K. Jacobson. 1995. Detection of temporary lateral confinement of membrane proteins using single-particle tracking analysis. *Biophys J*. 69:989-93.

Simson, R., B. Yang, S.E. Moore, P. Doherty, F.S. Walsh, and K.A. Jacobson. 1998. Structural mosaicism on the submicron scale in the plasma membrane. *Biophys J*. 74:297-308.

Singer, S.J. 1977. Thermodynamics, the structure of integral membrane proteins, and transport. *J Supramol Struct*. 6:313-23.

Singer, S.J., and G.L. Nicolson. 1972. The fluid mosaic model of the structure of cell membranes. *Science*. 175:720-31.

Sonnleitner, A., G.J. Schutz, and T. Schmidt. 1999. Free brownian motion of individual lipid molecules in biomembranes. *Biophys J*. 77:2638-42.

Soumpasis, D.M. 1983. Theoretical analysis of fluorescence photobleaching recovery experiments. *Biophys J*. 41:95-7.

Stahlhut, M., and B. van Deurs. 2000. Identification of filamin as a novel ligand for caveolin-1: evidence for the organization of caveolin-1-

associated membrane domains by the actin cytoskeleton. *Mol Biol Cell*. 11:325-37.

Stefanova, I., V. Horejsi, I.J. Ansotegui, W. Knapp, and H. Stockinger. 1991. GPI-anchored cell-surface molecules complexed to protein tyrosine kinases. *Science*. 254:1016-9.

Subczynski, W.K., and A. Kusumi. 2003. Dynamics of raft molecules in the cell and artificial membranes: approaches by pulse EPR spin labeling and single molecule optical microscopy. *Biochim Biophys Acta*. 1610:231-43.

Sun, F., M.J. Hug, C.M. Lewarchik, C.H. Yun, N.A. Bradbury, and R.A. Frizzell. 2000. E3KARP mediates the association of ezrin and protein kinase A with the cystic fibrosis transmembrane conductance regulator in airway cells. *J Biol Chem*. 275:29539-46.

Suter, D.M., L.D. Errante, V. Belotserkovsky, and P. Forscher. 1998. The Ig superfamily cell adhesion molecule, apCAM, mediates growth cone steering by substrate-cytoskeletal coupling. *J Cell Biol*. 141:227-40.

Suter, D.M., and P. Forscher. 2001. Transmission of growth cone traction force through apCAM-cytoskeletal linkages is regulated by Src family tyrosine kinase activity. *J Cell Biol*. 155:427-38.

Suzuki, K., F. Sanematsu, T. Fujiwara, M. Edidin, and A. Kusumi. 2002. Rapid diffusion of putative raft molecules indicative of the absence of large stable rafts in the resting-state cell membrane. *Biophysical Society Annual Meeting Abstracts*:348a.

Thompson, N.L., A.M. Lieto, and N.W. Allen. 2002. Recent advances in fluorescence correlation spectroscopy. *Curr Opin Struct Biol*. 12:634-41.

van Meer, G., and K. Simons. 1988. Lipid polarity and sorting in epithelial cells. *J Cell Biochem*. 36:51-8.

Van Regenmortel, M.H. 1998. Thermodynamic parameters in immunoassay. *Clin Chem Lab Med*. 36:353-4.

Watanabe, K., K. Saito, M. Kinjo, T. Matsuda, M. Tamura, S. Kon, T. Miyazaki, and T. Uede. 2004. Molecular dynamics of STAT3 on IL-6 signaling pathway in living cells. *Biochem Biophys Res Commun*. 324:1264-73.

Waugh, R.E., J. Song, S. Svetina, and B. Zeks. 1992. Local and nonlocal curvature elasticity in bilayer membranes by tether formation from lecithin vesicles. *Biophys J*. 61:974-82.

Yokosuka, T., K. Sakata-Sogawa, W. Kobayashi, M. Hiroshima, A. Hashimoto-Tane, M. Tokunaga, M.L. Dustin, and T. Saito. 2005. Newly

generated T cell receptor microclusters initiate and sustain T cell activation by recruitment of Zap70 and SLP-76. *Nat Immunol*.

Zacharias, D.A., J.D. Violin, A.C. Newton, and R.Y. Tsien. 2002. Partitioning of lipid-modified monomeric GFPs into membrane microdomains of live cells. *Science*. 296:913-6.

Zhang, F., W.G. Schmidt, Y. Hou, A.F. Williams, and K. Jacobson. 1992. Spontaneous incorporation of the glycosyl-phosphatidylinositol-linked protein Thy-1 into cell membranes. *Proc Natl Acad Sci U S A*. 89:5231-5.